

Chapter 2A

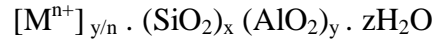
Review on zeolite supported ionic liquids in organic synthesis with special emphasis on preparation of 3, 4-dihydropyrimidinone derivatives via Biginelli reaction

2A.1. Zeolites: Composition and Structure

Zeolites are micro porous crystalline aluminosilicates, composed of infinitely extending three dimensional networks of $[\text{SiO}_4]^{4-}$ and $[\text{AlO}_4]^{5-}$ tetrahedra linked to each other by sharing of oxygen atoms between two T elements of TO_4 unit (T= Si, Al) [1]. The presence of Al^{3+} cation in SiO_2 framework makes the framework negatively charged, and requires additional extra framework inorganic/organic cations within the structure to keep the overall zeolite framework neutral.

The definition of zeolite is given by Smith [2] as “A zeolite is a crystalline aluminosilicate with a tetrahedral framework structure enclosing cavities occupied by cation and water molecules, both of which have enough freedom of movement to permit cation exchange and reversible dehydration”. The microporosity must be “open”, and the framework must have enough stability to allow the transfer of materials between interior and exterior of the crystals.

The composition of zeolites can be written in terms of three components such as extra framework cations, TO_4 framework and sorbed water molecule as follows:



Here M^{n+} is the exchangeable extra framework cation and gives rise to variety of ion-change materials. The value of $(x+y)$ indicates the total number of TO_4 per crystallographic unit cell. The x/y ratio of zeolite formulae is equivalent to the amount of Si/Al ratio per unit cell. The value of Si/Al lies in between 1 and ∞ . The composition of zeolite structure is found to depend on the synthesis condition. Further post synthetic modifications have been developed for insertion of Si or Al into the framework [3]. The hydrothermal and hydrophobic properties of zeolites structure increases as the ratio of Si/Al increases.

The primary building unit (PBU) of all types of zeolites is tetrahedra of four oxygen anions surrounding a silicon and aluminium ion (**Fig. 2A.1**). These tetrahedra are so arranged that each of the four oxygen anions is shared in turn with another silica or alumina tetrahedra. Lowenstein proposed [4] that no two Al atoms are joined together via Al-O-Al bond involving the same oxygen atom within the zeolite framework. Each silicon has +4 charge balanced by four tetrahedral oxygen and therefore silica tetrahedra are electrically neutral. Each alumina tetrahedron has a residual charge of -1 as it

bonded to four oxygen anions. Hence, each of the alumina tetrahedra requires a +1 charge from a cation in the structure to maintain electrical neutrality. These cations are usually sodium in the zeolites as it is initially prepared, but they can be readily replaced by ion exchange method. The oxygen at each tetrahedral corner is connected with another tetrahedron in straight line with the formation of T-O-T bridge (**Fig. 2A.1**). These PBU's are combined to form the secondary building units (SBU's) of the zeolite framework (**Fig.2A.2**) with unique topology [5].

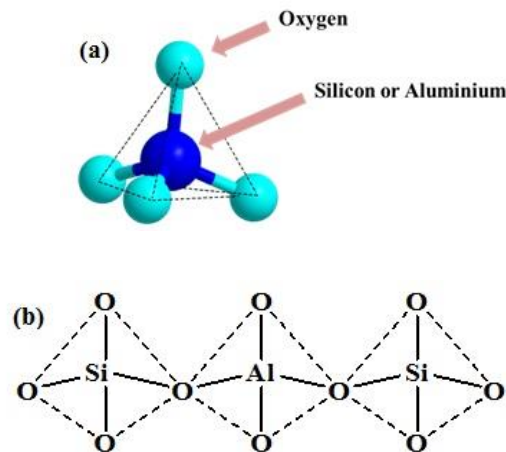


Fig. 2A.1: (a) Primary building unit of zeolite structures; (b) T-O-T bridge

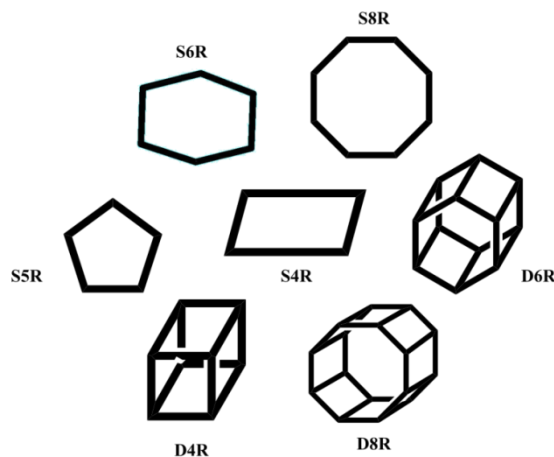


Fig. 2A.2: Secondary building unit of zeolite structures

As soon as SBU's are linked together, any geometrical shape like sodalite cage can be formed for the zeolite framework (**Fig.2A.3**). The SBU for each zeolite structure have been derived assuming that a zeolite network is composed entirely of one kind of unit. The wide variety of possible zeolite structures is the result of large numbers of ways in which the SBU can be linked to form various polyhedra. These polyhedra create networks of regular channels and cavities. The compositions of secondary building units

are different in different types of zeolites and within the zeolite structure; a unit cell always contains the same number of SBUs.

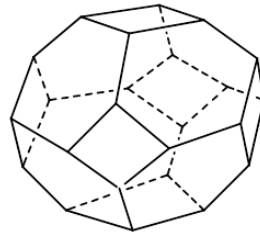


Fig. 2A.3: Sodalite cage structure (Tertiary building unit)

The truncated octahedron shapes of sodalite cage has 24 numbers of linked tetrahedra (T) and are further linked with distinct framework topology in different zeolites. Within the sodalite cage (also known β cage), they are interlinked through four and six membered rings.

The Structure Commission of the International Zeolite Association (IZA) assigns each zeolite framework with a three-letter mnemonic code based on the arrangement of SBUs (**Table 2A.1**) [6]. Some of the designations of SBUs structure types are FAU for the structure type of Faujasite zeolite, MFI for ZSM-5 zeolite, BEA for beta zeolite, MOR for mordenite type zeolites, LTA for zeolite A etc.

The microporous structures of zeolites depend on the size of oxygen ring that defines the pore size of the secondary building units. Therefore, it is necessary to give brief description of a zeolite structure in terms of specific pore opening and dimension of the channel system within the structure.

Table 2A.1: Examples of nanoporous aluminosilicates with their three letter IZA designation and description of the pore systems

System	Pore system
Sodalite family (SOD) (e.g. mineral and synthetic sodalities)	3-dimensional; 6-ring channels
Zeolite A family (LTA) (e.g. zeolites A, ZK-4; no mineral analogue)	3-dimensional; 8-ring channels
Chabazites (CHA) (e.g. mineral chabasites, SSZ-13)	3-dimensional; 8-ring channels

ZSM-5 (MFI) (e.g. mineral murataite, silicalite)	2-dimensional; 10-ring channels
Ferrierites (FER) (e.g. mineral and synthetic ferrierites)	2-dimensional; 10 & 8-ring channels
Faujasites (FAU) (e.g. mineral faujasites, zeolites LSX, X, Y, US-Y)	3-dimensional; 12-ring channels

2A.2. Classification of zeolites

Zeolites can be classified based on their morphological characteristics, chemical composition, effective pore diameter and natural occurrence.

Bragg [7] first made the classification based on morphological characteristics. According to this, zeolites are classified as fibrous, lamellar and those having framework structures. It was later modified by Meier and Barrer according to the SBU's present in them.

Zeolites are divided into three groups based on their pore size, number of tetrahedra and maximum free diameter within the pores (**Table 2A.2**) [8, 9].

Zeolites can also be classified into three classes according to their Si/Al ratio [10], namely:

- Zeolites with low Si/Al ratios (<5): e.g., Zeolite A, Zeolite X, Zeolite Y
- Zeolites with medium Si/Al ratios (5 to 10): e.g., Mordenite
- Zeolites with high Si/Al ratios (>10): e.g., ZSM-5

The thermal stability increases from about 700 °C in low silica zeolites to about 1300 °C in high silica zeolites.

Table 2A.2: Classification of zeolites

Type	No of tetrahedra	Pore diameter of framework (O) (Å)	Examples
Small pore size	8	Diameter (O) $\leq 4.5 \text{ \AA}$	Zeolite A
Medium size	10	$4.5 \text{ \AA} < \text{diameter (O)} \leq 6.5 \text{ \AA}$	ZSM-5(pentasil)

			type)
Large pore size	12	Diameter(O) > 6.5 Å	Zeolite Y(Faujasite type)

2A.3. Characteristic properties of zeolites

The properties of a zeolite are dependent on the topology of its framework, the size, shape and accessibility of its free channels, the location of charge and size of the cations within the framework, the presence of impurities, the ordering and local environment of T-atoms. They have a microporous crystalline framework and are more commonly known as molecular sieves. Zeolites have some interesting structural properties which can be listed as below:

- (a) High hydrothermal and mechanical stability
- (b) Defined porous structure lying in the range of common chemicals with high surface area: it gives rise to shape selectivity effect in adsorption process
- (c) Tunable chemical composition: The constituent positive cations of zeolite framework are rather loosely held and can be exchanged for others in contact solution.
- (d) High sorption capacity due to high porosity: It allows molecules of adsorptive as well as reactants, products or transition states of chemical reactions to be selectively excluded from access to and/or egress from the zeolite pores [11].
 - (e) Environment friendly.
 - (f) Recoverable and reusable.

These properties make zeolites attractive candidates for several purposes such as gas adsorption processes, development of heterogeneous catalytic systems, ion-exchange reactions etc. Zeolites are often preferred as support materials over other mesoporous materials without crystalline framework. Since a support material may sometimes exert structural effect brought about by its textural and active phase-linked effect, hence it must possess certain properties like porosity, surface area, dispersion, selectivity and of course activity. Zeolites in this context, successfully justify the requirements. The synergistic effect of the morphology, porosity of the zeolite structure

and catalytic ability of the supported phase results in to development of a heterogeneous catalyst with high thermal as well as chemical stability and activity.

2A.4. Structure of Y Zeolite

Zeolite Y has the faujasite framework structure with sodalite cages as the tertiary building units (TBU) (**Fig.2A. 3**). In this, the tetrahedra are linked to form cubooctahedra or so-called β cage units. The β -cage has both four-membered and six-membered rings in its structure. Zeolite A is formed by bridging (not fusing) the four-membered rings in its structure. Zeolite X is formed by bridging (not fusing) the six-membered rings. It does not occur in nature, but is industrially produced on a massive scale for its use in ion exchange, gas separation and drying processes. If the six-membered rings are bridged, then possibly the most important zeolite structure, zeolite X/Y is formed. Depending on the silica-to-alumina ratio of their framework, synthetic faujasite zeolites are divided into X and Y zeolites. The Si/Al ratios are 1-1.5 for the X zeolite and 1.5-3 for the Y zeolite. The unit cell of the faujasite type zeolites is cubic with a unit cell dimension of 25\AA and it contains 192 silica and alumina tetrahedra. Each of the sodalite unit is connected to four other sodalite units by six bridging oxygen atoms connecting the hexagonal faces of two units to generate layers of sodalite units. The oxygen bridging unit is referred to as the hexagonal prism. The sodalite layers are also linked by hexagonal prisms in an ABC sequence to generate a tetrahedral array of sodalite having cubic symmetry and the same space group as diamond. This arrangement of sodalite units generates wide pores with free diameter of $7\text{-}8\text{\AA}$ via the interlinking of 12 tetrahedra, which provides entrance in to larger supercages of $11\text{-}12\text{\AA}$ diameter. The supercages are linked tetrahedrally via the 12 rings to form a highly porous framework structure [12]. Owing to the large microporous spaces, Zeolite Y (**Fig. 2A.4**) has the liberty to allow organic molecules to diffuse in and out easily from the framework. This property makes zeolite very useful for catalytic, ion-exchange and absorption purposes.

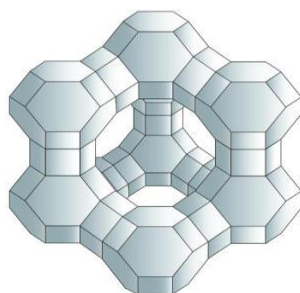


Fig. 2A.4: Cage structure of Y zeolite

2A.5. Dealumination of Y zeolite

The term “dealumination” refers to structural modification of zeolite frameworks with formation of extra framework aluminium species (EFAl) by chemical reactions resulting in deficiencies of framework Al lattice points [13]. The various important parameters of zeolite can be affected with variation of the ratio of framework Si/Al atoms within the zeolite structure using chemical and hydrothermal treatments. Mainly, this ratio exerts a strong influence on the physical properties such as maximum ion-exchange capacity, hydrothermal and thermal stability, hydrophobic properties, and generation of strong Brönsted-acidic sites which may determine the catalytic activity and selectivity of modified form of zeolite structure for a particular reaction. Since the low Si/Al ratios zeolite are unstable in acids or water at elevated temperatures, therefore zeolites with low aluminum content (high Si/Al ratio) are more favorable, especially when applied as catalysts [14-16]. The commercial synthesis of faujasite family (X & Y) cannot be directly obtained with the Si/Al ratios substantially higher than 3 [17]. Therefore, all catalytically relevant material must be prepared by post synthetic removal of framework Al that can increase the Si/Al ratio to thermally stable dealuminated zeolite. Generally, the dealumination process of zeolite framework can be divided into three categories such as (1) those involving removal of framework aluminium by chemical agents or by thermal dehydroxylation, (2) those in which in addition to the mere extraction of framework aluminium, framework vacancies are filled by intrinsic silicon and oxygen atoms migrating in the zeolite lattice by hydrothermal treatment and (3) those representing true substitution reactions of Al component of the framework and the dealuminating agent. Not all zeolites can preserve the integrity of the framework during dealumination process. The structural arrangement and stability of the framework may get compromised depending upon the severity of the conditions applied.

The first synthesis of Y-zeolite was reported by Breck [18] in 1964 and he observed that the change of X to Y modifications occurs at a critical characteristic value of Si/Al ratio at 1.5. Ruster et al. [19] in 2006 described another typical chemical behavior of the Y-zeolite sample that is dealumination by steam treatment. According to that observation, Y zeolite may be dealuminated in steam above the Si/Al ratio of 2.2 without destruction of its framework. At the same time, NaA and NaX zeolites get completely collapsed after any dealumination process. Different dealumination

techniques of Y-zeolites include acid extraction [20], isomorphous Al/Si substitution [21] and thermochemical treatment of NH_4Y [22]. The healing effects of NH_4Y in dry or wet air were also investigated by Ward in 1972 that led to structural features of dealuminated Y zeolites (DAY) [23]. The appearance of EFAl species brings a stabilizing effect on the zeolite framework with a more regular structure in the DAY zeolite [24]. The higher thermal stability of DAY samples were reasoned for removal of mineralizing effects of Na^+ ion on the destabilization of framework [25], preferential formation of Si-O-Si bonds as a results of dehydroxylation of intermediately formed hydroxyl nests [26] and also healing effects of Al defects with migration of H_4SiO_4 from the crystal surface [27]. Different types of defects such as sorption centers for gases or liquids are reorganized in the form of regular structure and thus the silica framework loses its sorption behavior with rising temperature [28]. The formation of secondary pore structure in DAY is one of the reasons for higher activity of the zeolite in high temperature catalytic process.

The dealumination process of Y-zeolite favors the formation of an ultra-stable Y-type zeolite (USY). It makes it so by drastically improving the thermal as well as chemical stability of the zeolite framework. Mild hydrothermal treatment of the faujasite type Y-zeolite usually triggers partial release of aluminium from the zeolite framework and results in to formation of extra-framework aluminium species. The oxoaluminum cations, such as AlO^+ , AlOH_2^+ , and $\text{Al}(\text{OH})_2^+$, and some neutral species such as AlOOH and $\text{Al}(\text{OH})_3$ are proposed to be the EFAl species. The presence of these EFAl species improves not only the thermal stability but also the catalytic activity of the dealuminated zeolite framework. This beneficial effect of EFAl species on the catalytic activity can be understood on the basis three hypotheses: (a) some EFAl species themselves serve as the Lewis acidic site; (b) their presence stabilizes the negative charges on the lattice after removal of the acidic protons; (c) there is synergistic effect between the EFAl species and the nearby Brönsted acidic sites thereby resulting in to formation of super acidic zeolite framework [29].

All these three hypotheses are the outcome of extensive studies by the researchers on the dealumination of Y-zeolite framework from time to time. Though these hypotheses are largely debated [30, 31], some researchers have proven their point based on sound experimental evidences as well as theoretical calculations [29]. The resulting super acidity of the dealuminated of Y-zeolite framework was also reasoned to

the interactions between protonic sites and polymeric oxoaluminium deposited in the zeolite voids [32] and can be very beneficial for promoting isomerization, cracking, hydrogen transfer in dealuminated HY framework as well as acid catalyzed organic conversions [33, 34].

2A.6. Use of zeolite as support material for immobilization of ionic liquids

The immobilization of ILs on to a solid support provides a simple way for reducing the amount of IL required for a given application, reducing accordingly the associated cost; simplifies their handling and separation process from the reaction mixture, and finally, significantly reduces the leaching of ILs to the environment [35]. Among various types of inorganic supports (e.g. alumina, silica, clay etc.), zeolites have some unique properties for efficient immobilization of ILs on their surfaces such as high surface area, well organized pore channels, excellent thermal stability, environmentally benign nature and high absorption towards organic compounds [36]. There are a few reports found in literature on the synthesis of zeolite supported ionic liquids and their use in different organic syntheses as heterogeneous catalyst. The supported IL material can manifest good thermal and water stability as compared to the parent IL. The immobilization of the ionic liquid can be achieved by different means, such as by covalent anchoring of the surface functional groups with the cation or anion of the ionic liquid or without covalent bonds in the form of supported liquid phases. In some cases up to minimal loading of 10%, small islands of the ionic liquid could form over the support material; while in cases of high loading complete coverage of the support surface occurred.

The heterogenization of acidic ionic liquids on solid supports offers several advantages as compared to the use of catalytically active ILs in homogeneous or heterogeneous phases. The number of accessible active sites of the catalyst may increase through immobilization and thus reduction in the amount of IL required for catalysis. The leaching problem of IL phase is completely eliminated in the covalent attachment mode. It is suitable for application in a continuous fixed bed reactor.

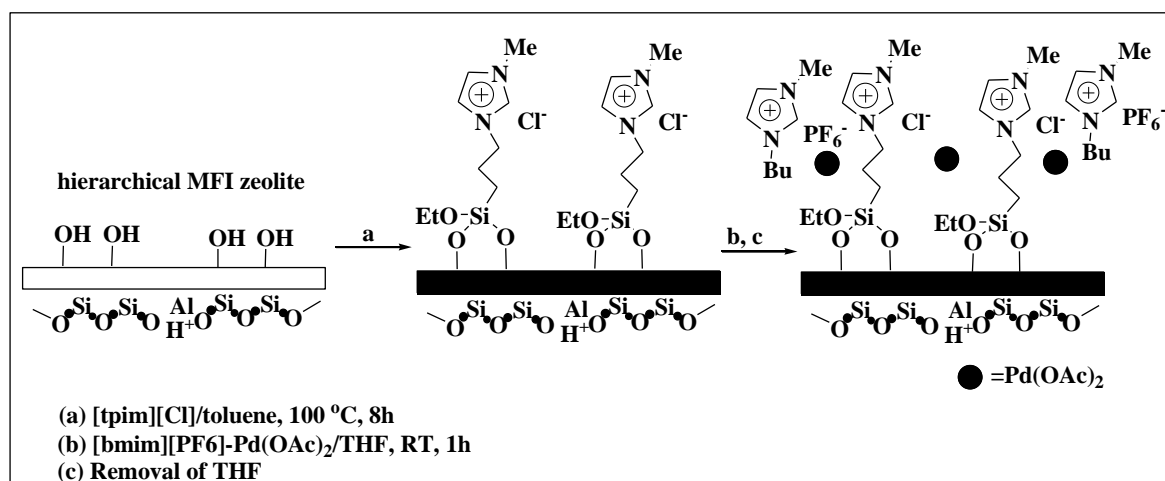
This section summarizes the literature for immobilization of ionic liquids on zeolite support and their utilization in organic synthesis as well as in other fields till 2016.

DeCastro et al. [37] prepared immobilized Lewis acidic ionic liquids (AL-ILs) in different ratios of 1-butyl-3-methyl-imidazolium chloride ([bmim]Cl) and AlCl_3 on SiO_2 , Al_2O_3 , TiO_2 , ZrO_2 and H-BEA zeolite ($\text{Si}/\text{Al} = 13.8$) in order to prepare heterogeneous acidic catalysts for the alkylation of aromatic compounds with dodecene under continuous liquid-phase and continuous gas-phase batch methods. A comparison of catalytic activities of different supports expressed higher activity of silica-based supports in the alkylation reaction of benzene with dodecene. In this study, the zeolite based IL material was not selected for studying the alkylation reaction, since the zeolite structure significantly lost its crystallinity after immobilization of AL-IL. The shape-selective effects of pure beta-zeolite towards generation of 2-phenyl-dodecane product were lost in case of the AL-IL supported beta-zeolite under the same reaction condition.

Valkenberg et al. [38] prepared supported Lewis-acid catalysts for Friedel-Crafts reaction by immobilizing chloroaluminate ionic liquids in different porous materials such as silica, alumina, MCM-41, NaY zeolite, Nb_2O_5 and TiO_2 . The ILs were added directly on to the porous support without use of any solvent. These materials containing ionic liquids in supported phase showed leaching of the IL components in liquid phase reactions. The major drawback of this method was observed in case of the structured support materials, namely zeolites and MCM-41. The structure of the supports was destroyed after immobilization of chloroaluminate ionic liquids as evidenced in PXRD analysis [39-41].

Pietschmann et al. [39] impregnated $[\text{EMIM}^+][\text{BF}_4^-]$ over BEA zeolite and mesoporous silica by addition of zeolite powder (or silica powder) in to a solution of IL in methanol under continuous stirring for several hours. The solid materials were separated from the suspension by filtration and any excess of IL was removed by Soxhlet extraction.

Jin et al. [42] immobilized palladium acetate in thin ionic liquid layers on the mesopore wall of hierarchical MFI zeolite (**Scheme 2A.1**) and examined as heterogeneous catalyst for Suzuki coupling reaction in water. The catalyst exhibited very high activity in the coupling of various aryl bromides with aryl boronic acids in water with high stability. This catalyst could be recycled for four runs without significant loss in catalytic activity. Hierarchical MFI zeolite was proven to be a promising support for the supported ionic liquid catalysis.



Scheme 2A.1: Synthesis of MFI-supported Pd(OAc)₂-ionic liquid

Ntais et al. [43] studied the synthesis of NaY zeolite-ionic liquid (H-3-methylimidazolium bis(trifluoromethanesulfonyl) imide) (HMITFSI) composites with a weight ratio of IL/Zeolite = 250 and the excess of IL was eliminated from the composite material by Soxhlet extraction. The prepared material was characterized via Powder XRD analysis and FT-Raman spectroscopy. The XRD patterns showed a redistribution of extra framework cations without loss in crystallinity of the zeolite structure. This study indicated encapsulation of HMITFSI in to the zeolite pores and that HMI⁺ might have replaced part of the Na⁺ in the zeolite structure. The FT-Raman spectra of the composite supported the presence of both the two ions of the ionic liquid even after 24 hours of Soxhlet extraction.

Ntais et al. [44] synthesized H-3-methylimidazolium bis(trifluoromethane sulfonyl)imide encapsulated NaY zeolite composites (TFSI)/NaY with six different weight ratios of IL/zeolite and studied their ion transport properties. The different properties of the resultant composites showed direct correlation of the loaded ionic liquid amount over the zeolite. The composites displayed lower water capacitance with increasing loading of IL because of reduction of the micro pore surface area. Likewise, the A.C. impedance measurement revealed that at dry condition, conductivity of the composites increased with loading and temperature. However, measurements at wet conditions revealed two different temperatures dependencies. At higher IL loading, the conductivity increased with increasing temperatures while the opposite was observed for lower IL loaded composites.

Eguizábal et al. [45] developed supported ammonium based ionic liquid systems (2-hydroxymethyl)trimethylammonium dimethyl phosphate (IL1) and N,N-dimethyl-N-(2-hydroxyethyl) ammonium bis(trifluoromethanesulfonyl) imide (IL2) with Y (FAU framework code) and beta (BEA framework code) type zeolites for evaluation of proton transfer conduction properties of the composites. These composites were used as raw materials in high temperature proton exchange membrane fuel cells (HTPEMFCs) (**Fig. 2A.5**). The encapsulation of ILs in the support was confirmed with the help of X-ray diffraction, N₂ physisorption, TGA analysis, ATR-FTIR, Raman spectroscopy and A.C. impedance measurement techniques. The conduction properties of the composites as a function of temperature and water partial pressure have been selected as analytical tool to define the best encapsulation procedure and hence to develop IL/Zeolite composites for proton exchange membrane fuel cell (PEMFC) applications.

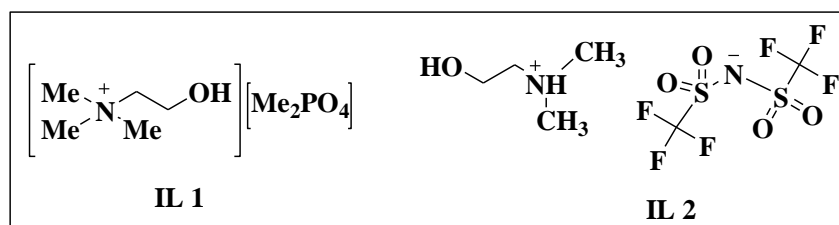
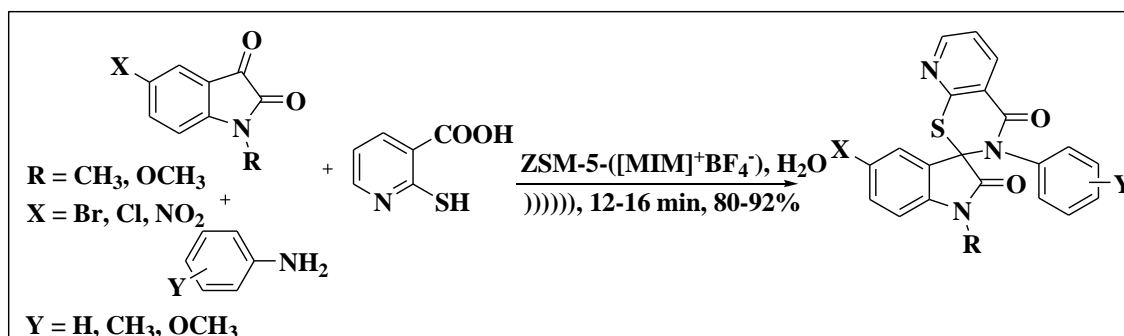


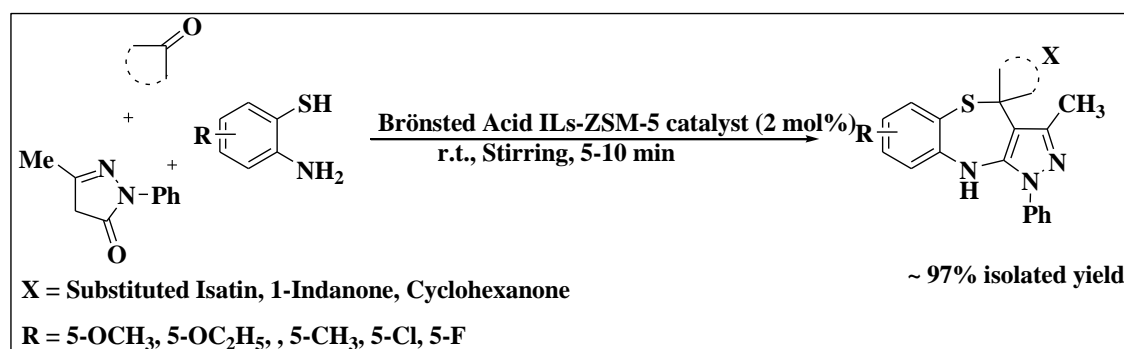
Fig. 2A.5: Structure of ammonium based ILs

Arya et al. [46] developed Brønsted-acidic catalyst systems by supporting Brønsted acidic ionic liquids 1-methylimidazolium tetrafluoroborate ionic [MIM][BF₄] over ZSM-5 zeolite. The catalytic efficiency of the synthesized Supported Ionic Liquid Phase (SILP) materials were examined for the preparation of spiro[indole-pyrido[3,2-e]thiazine] in water under ultrasonic irradiation (**Scheme 2A.2**). The reactions were also studied under conventional heating and microwave promoted conditions. The ultrasound-promoted method proved to be more efficient in terms of product yield. The recyclability of the catalytic system was tested under ultrasound-promoted reaction condition and it was found that the catalytic system could be easily recycled up to fifth consecutive cycles without any obvious loss in activity.



Scheme 2A.2: Synthesis of spiro[N-substituted indole-pyrido thiazines]

Arya and Prabhakar [47] encapsulated 10 mol % of various ionic liquids namely ([Bmim][BF₄], [Bmim][PF₆], [C₈mim][BF₄] and [C₈mim][PF₆]) within mesoporous ZSM-5 zeolite on the basis of organic-additive -instant seed technology method [48]. The catalytic activity of the synthesized systems was tested for the synthesis of spiro[pyrazolo[3,4-e]benzothiazepine] analogues in water within short reaction time (**Scheme 2A.3**). The recyclability profile of the [Bmim][BF₄] confined ZSM-5 zeolite system was checked and it was found to be successfully recycled for six consecutive cycles without any appreciable loss in catalytic activity.



Scheme 2A.3: Synthesis of spiro [pyrazolo[3,4-e][1,5]benzothiazepine] analogues

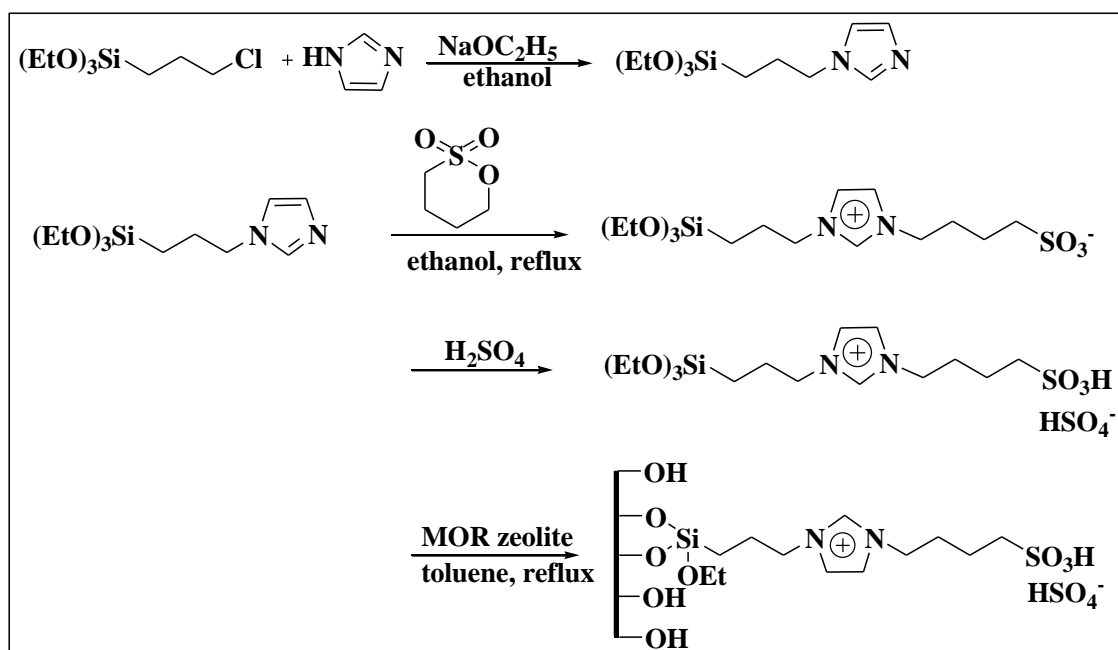
Noroozifar et al. constructed [49] a novel biosensor by incorporating modified nanosized natural zeolite and 3-hydroxypropanaminium acetate (HPAA) as a novel room temperature ionic liquid, supported on multiwalled carbon nanotube (MWCNTs) and employed for the simultaneous determination of dopamine (DA) and uric acid (UA).

Blanes et al. [50] introduced an approach for generation of three different zeolite families (BEA, MFI, and ANA) using 1-butyl-3-methyl imidazolium methane sulfonate [bmim][CH₃SO₃] as template. The use of TEOS (Tetraethyl orthosilicate) as a silicon source and [bmim][CH₃SO₃] as a templating agent results in IL/Na-ZSM-5 composite

with the IL remaining trapped within the zeolite structure. The encapsulated IL acquires a configuration where the longer alkyl chain of substituted imidazolium enters the secondary cages of the structure. The resulting ionic liquid-zeolite composite showed resistance towards high thermal treatment supporting either the chemical bonding through the imidazolium ring to the zeolite framework (bmim-BEA) or the entrapment of the IL into the resulting channels (bmim-MFI). The replacement of the silicon source by colloidal silica led to the formation of IL/BEA composite with IL playing the role of the charge compensation cation. The sole mordenite structure was obtained in absence of the IL.

Yu et al. [51] developed a ship-in-a-bottle strategy to prepare [APMIM]Br@NaY host-guest system for CO₂ capture from simulated flue gas. The host-guest system was prepared by in situ encapsulation of 1-aminopropyl-3-methylimidazolium bromide ([APMIM]Br) IL in the NaY supercages. The encapsulated ILs were found to be more stable than the bulk ILs. The excellent physicochemical properties and the CO₂ capture performance of the host-guest systems render great pledge for the future practice in the industrial CO₂ capture.

Li et al. [52] synthesized a heterogeneous mordenite (MOR) supported Brønsted acidic IL catalyst: BAIL@MOR via covalent anchoring of [CPES-BSIM]-[HSO₄] ionic liquid over mordenite zeolite (**Scheme 2A.4**). The covalent binding interactions of the BAIL [CPES-BSIM][HSO₄] was confirmed from the combined characterization results of XRD, FT-IR, SEM, TG-DTG and N₂ adsorption isotherm studies. The prepared material was investigated as efficient recyclable catalyst in the ketalization of cyclohexanone with 1, 2-propylene glycol and 1, 3-butylene glycol under mild reaction conditions. The conversion of the cyclohexanone showed positive dependence with the reaction temperature and catalyst loading in the presence of BAIL@MOR as catalyst. The catalyst witnessed a very good recyclability profile up to five consecutive cycles.



Scheme 2A.4: Route for the synthesis of catalyst BAIL@MOR

Losch et al. [53] explored the catalytic activity of [bmim][CH₃SO₃]/zeolite composites as heterogeneous catalyst in liquid phase toluene chlorination reactions. ILs/zeolites composites exhibited low toluene conversion at room temperature compared to the bare Na-zeolite. It may be reasoned to the restricted accessibility of the Na-zeolite pores in the presence of IL.

2A.7. Biginelli reaction: An introductory note

Biginelli is a kind of multicomponent reaction and it employs the easily accessible ethyl acetoacetate, aryl aldehyde and urea/thiourea to form the respective 3, 4-dihydropyrimidin-2(1H)-one (DHPM) derivatives. The reaction was named after Pietro Biginelli who had discovered it in 1893. He investigated the reaction of ethyl acetoacetate and urea in presence of benzaldehyde in EtOH under reflux conditions. The mechanism of Biginelli reaction has been a topic of much debate in various experimental and theoretical reports. As depicted in **Fig. 2A.6**, three main mechanisms involving the protonated intermediates have been proposed. The first mechanism which is called the iminium route, involves condensation between aldehyde and urea to give rise to an iminium intermediate, which further undergoes a nucleophilic addition with a β -keto ester resulting the DHPM. The second mechanism also termed as ‘enamine route’ is based on condensation between urea and β -keto ester leading to a protonated enamine intermediate, which subsequently reacts with aldehyde to form the DHPM. The

third mechanism involves a Knoevenagel type reaction mechanism. The reaction between aldehyde and β -keto ester results in the formation of a carbenium ion intermediate which further reaction with urea results the DHPM [54]. However, further studies confirmed the authentic route to be the iminium pathway [55-57].

After more than 100 years of long discovery, the reaction has still elicited due to diverse applications of the resulting product across therapeutic and pharmaceutical field. The traditional Biginelli reaction involves the use of strong acidic conditions to give the DHPMs. However, it suffers from low yield of the resulting product. The growing interest in DHPMs has surged interest in development of efficient routes and catalysts over the years. The search led to wide variations in reactions conditions. The use of different type of catalysts such as Brønsted/Lewis acidic, biocatalysts, heterogeneous catalysts, organocatalysts etc. was reviewed by Suresh and Sandhu in 2012 [58]. Recent developments also involved the use of environment friendly and easily recoverable nanocatalysts to carry out the Biginelli reaction [59-62]. The blooming of different green protocols on account of growing interest over development of safer chemistry such as use of solvent free conditions, microwave heating, sonochemistry, use of water/ethanol as the solvent, ionic liquids etc. over the decades has been reviewed by Panda and co-workers in 2012 [63]. A recent review by Nagarajaiah and co-workers (2016) summarizes the critical developments of this reaction in the realm of material chemistry, natural product synthesis and also the access provided by this reaction towards syntheses of chiral DHPMs [54].

Considering the facile synthetic access provided by this reaction towards the diverse heterocyclic systems, researchers are still in to it and the outcome is exciting research publications in peer-reviewed journals with variation in every possible manner.

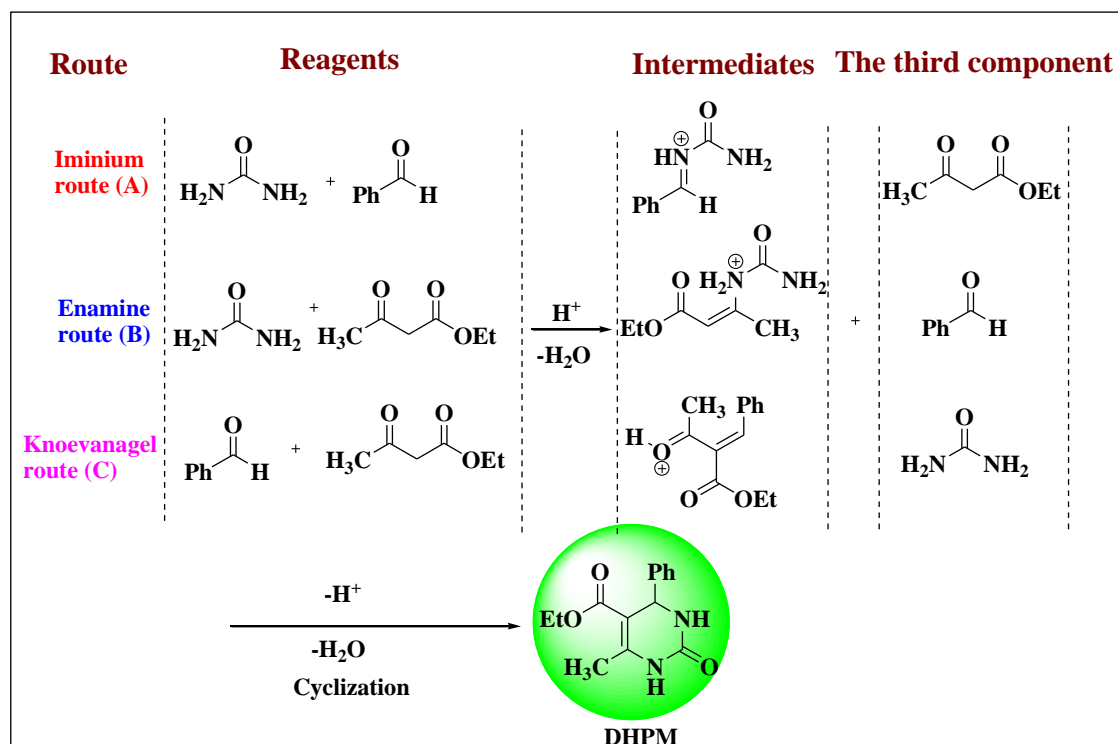


Fig. 2A.6: Mechanisms for Biginelli reaction

2A.8. Biological aspects of Biginelli 3, 4-dihydropyrimidinone (DHPM) derivatives

Biginelli DHPMs possess wide spectrum of interesting pharmaceutical and therapeutic activities. After Pietro Biginelli discovered the multicomponent route to the multifunctionalized dihydropyrimidinones in 1893, these partly reduced pyrimidines were largely ignored in the following decades and hence the biological activity of these compounds remained unexplored. For the first time in 1930, the wool protection activity of these scaffolds was patented [58]. Since the early 1980s, the interest in dihydropyrimidinones surged due to their apparent structural similarity to the well-known dihydropyridine calcium channel modulators of the Hantzsch type: nifedipine (**1**); the respective biginelli product being an aza-analogue (**2**) proved to be an effective orally active antihypertensive agent [64] (**Fig. 2A.7**).

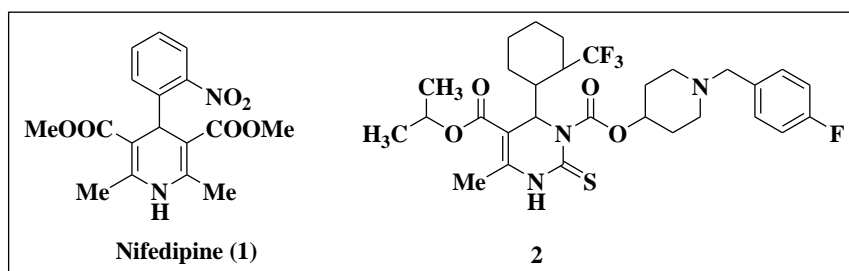


Fig. 2A.7: Structure of Nifedipine (1) and its biginelli analogue (2)

More recently, the interest has been shifted from DHPM calcium modulators to the development of other biologically active DHPM derivatives (**Fig. 2A.8**). DHPMs with annulated benzimidazole ring (**3**) showed potential potassium channel antagonists activity [65]. Also, Batzelladine A (**4**) derivative of DHPMs obtained from marine natural source have promising anti HIV activity [66]. Monastrol (**5**) was the first Biginelli compound which showed excellent anticancer activity [67]. Some other important pharmacological activities offered by DHPM derivatives are anti-epilepsy activity [68], anti-malarial activity [69], anti-microbial activity [70], anti-inflammatory activity [71], anti-tubercular activity [72] and anti-bacterial activity [73] etc. Additionally, some DHPMs are also developed as anti-oxidants [74], anti-filarial agents [75] and α -1A adrenergic receptor antagonists [76] in recent times. Apart from this, they are also employed as important agents for treating anxiety [77] and optic nerve dysfunction [78].

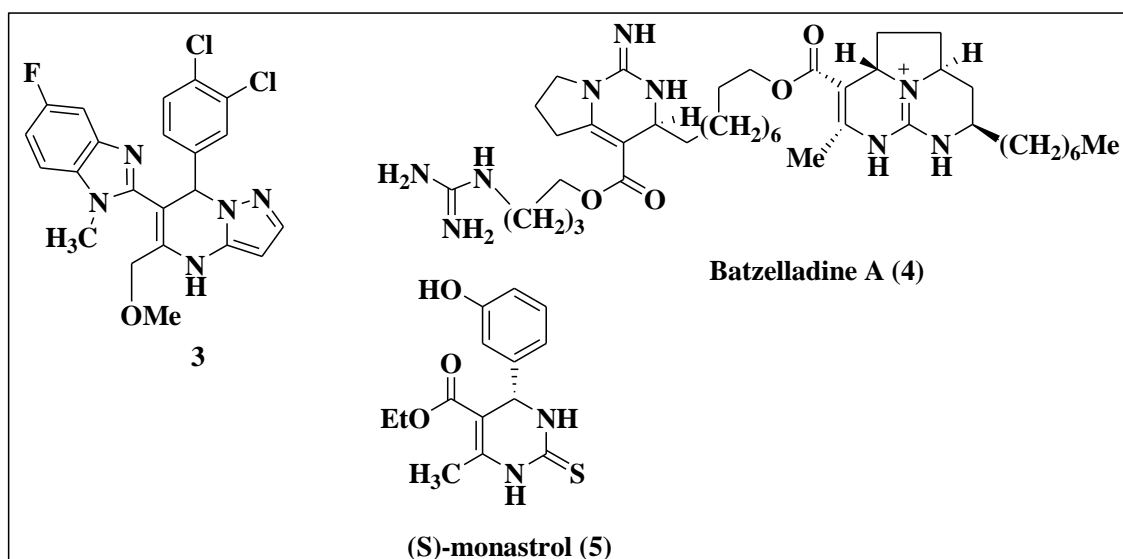


Fig. 2A.8: Structure of some important DHPM derivatives

These reasons led researchers to focus their attention on the synthesis of these compounds, to explore more and more functionalized DHPM derivatives and build up a rich library of potential agents suitable for different purposes.

The next section summarizes the literature on use of different heterogenized ionic liquid catalyst for development of 3, 4-dihydropyrimidinone derivatives over the years.

2A.9. Use of heterogenized ionic liquid catalysts for synthesis of 3, 4-dihydropyrimidinone derivatives via Biginelli reaction

In 2005, Wang et al. [79] studied the three-component Biginelli reaction of aromatic aldehyde, ethyl acetate and urea in glacial acetic acid at 100 °C using 3.5 mol% of polymer supported catalyst PsMimPF₆ (**Fig. 2A.9**) to afford the corresponding pyrimidine-5-carboxylates in yields up to 99% within 2 hour. The catalyst was prepared through immobilization of room temperature ionic liquids on polymer support which was reused at least five times with retention of original catalytic activity. Aliphatic aldehyde was not suited with this condition for the formation of Biginelli product.

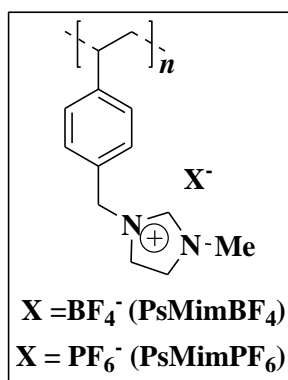
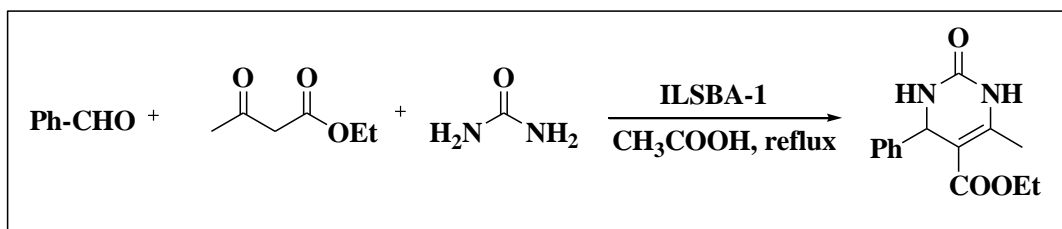


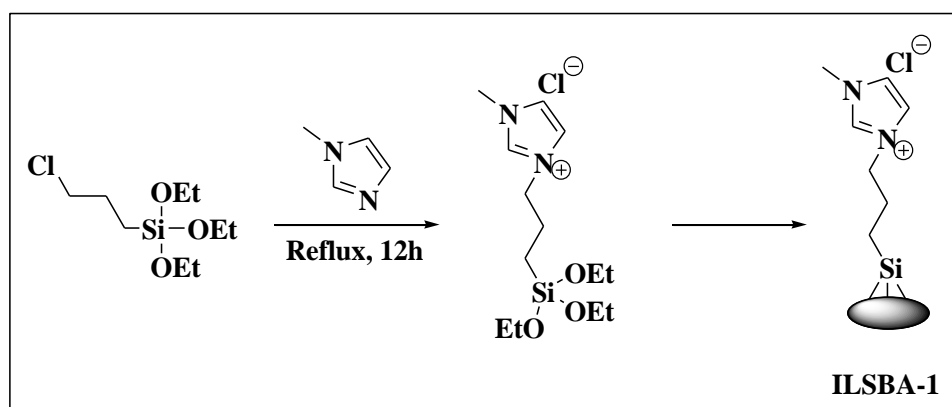
Fig. 2A.9: Structure of PsMimPF₆ and PsMimBF₄

The use of ionic liquid-functionalized SBA-15 (ILSBA-1) as catalyst in the Biginelli reaction was studied by Xu et al. [80] in three different solvents CH₃CN, EtOH and AcOH under reflux temperature according to the reaction **Scheme 2A.5**. It was observed that glacial AcOH was a better solvent with excellent isolated yield, and no precipitation was observed during reaction except for ILSBA-1. This catalytic system produced 59-95% yield of 3, 4-dihydropyrimidinone derivatives in presence of 1-5 mol % of catalyst within 3 hour reaction at 100 °C from various substituted aromatic

aldehydes. The ILSBA-1 catalyst was recycled for five times with good catalytic activities. The ionic liquid-functionalized SBA-15 (ILSBA-1) was prepared from MTESPIImCl (1-Methyl-3-[(triethoxysilyl) propyl]imidazolium chloride) by following the reaction **Scheme 2A.6** [81].

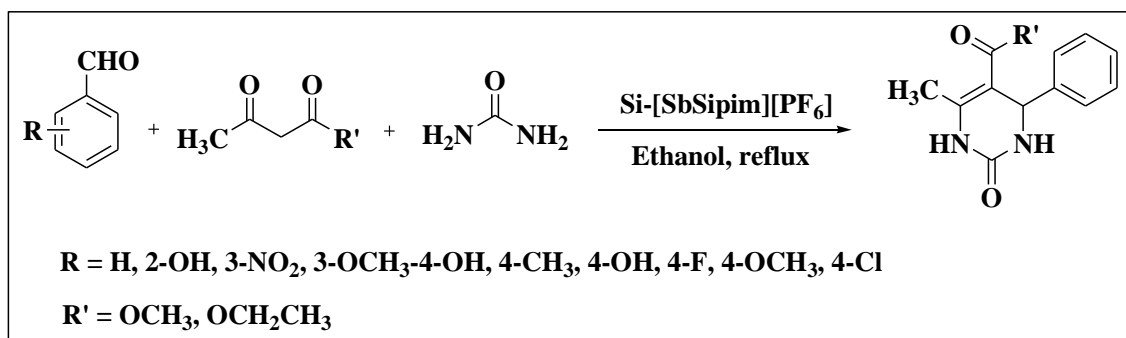


Scheme 2A.5: Synthesis of substituted tetrahydropyrimidine-5-carboxylates

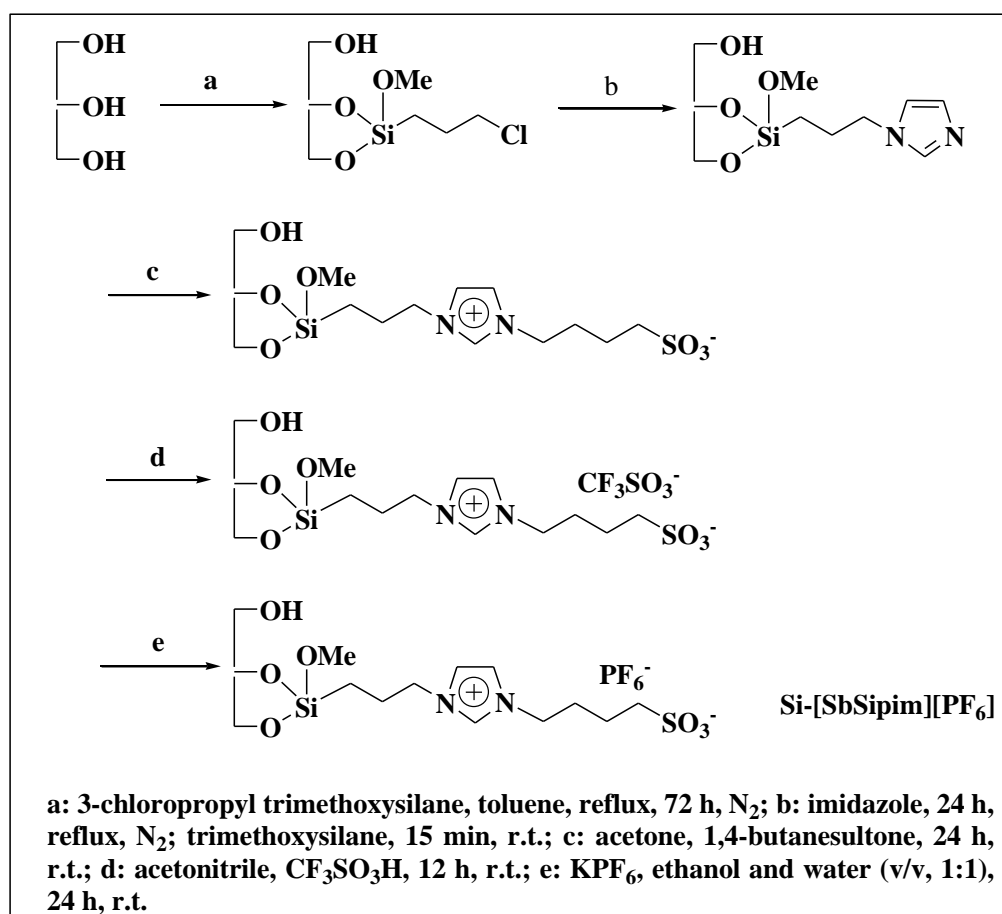


Scheme 2A.6: Synthetic route of MPIImCl-SBA (ILSBA-1)

Kang et al. [82] reported the use of silica-supported sulfonic acid-functionalized ionic liquid (Si-[SbSipim][PF₆]) as heterogeneous recyclable catalyst for the multi-component synthesis of Biginelli products. The reactions were carried out under reflux condition in ethanol within 3.5-5 hour to form 80-94 % yields of DHPM derivatives starting from various substituted aromatic aldehydes (**Scheme 2A.7**). The catalyst could be easily separated from the reaction mixture and efficiently reused for six times. The supported catalyst was prepared according to **Scheme 2A.8** [83].

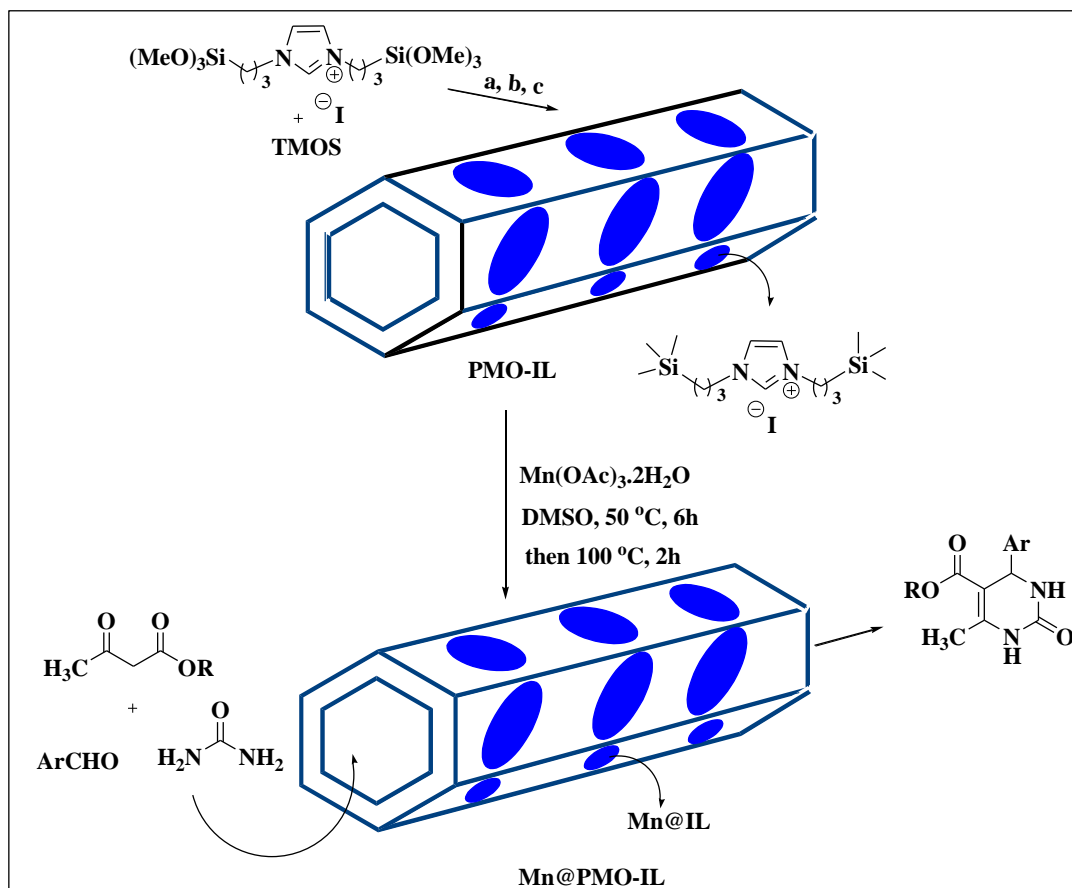


Scheme 2A.7: Synthesis of DHPM derivatives using Si-[SbSipim][PF₆] as catalyst



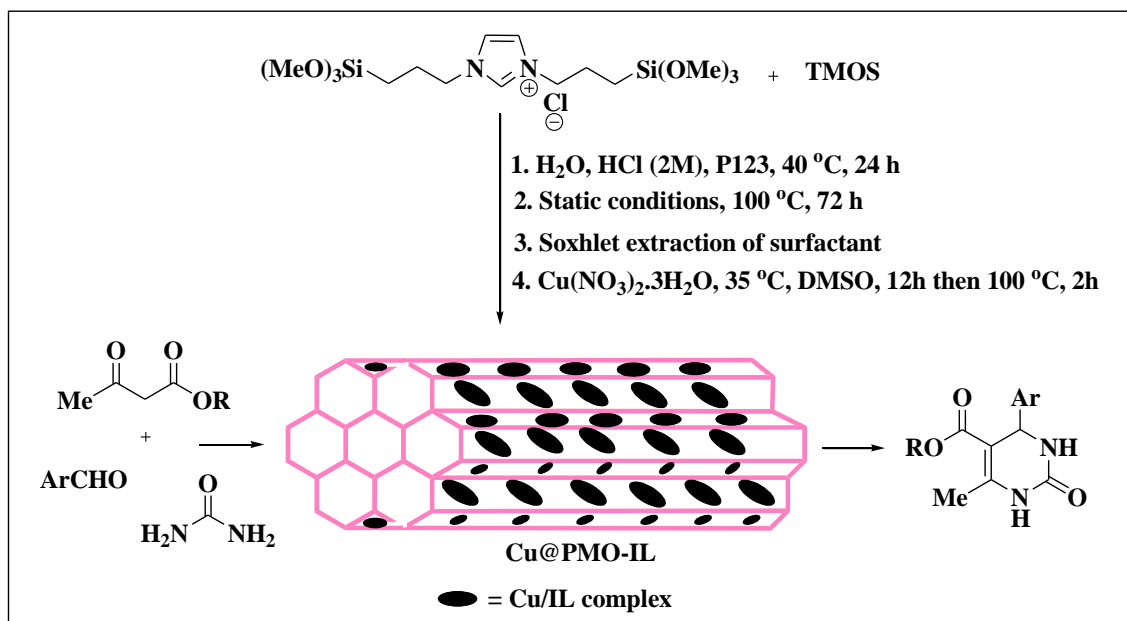
Scheme 2A.8: Synthetic route for Si-[SbSipim][PF₆]

Elhamifar and Shàbani [84] reported the catalytic application of manganese containing periodic mesoporous organosilica with ionic liquid framework (Mn@PMO-IL) in the synthesis of 3, 4-dihydropyrimidinones from the reaction of various aldehydes with urea and alkyl acetoacetates under solvent-free condition (**Scheme 2A.9**). The products were obtained within 45-120 min of duration in excellent yields with 0.6 mol% of catalyst at 75 °C. The catalyst was recovered and reused up to 14 times without significant loss in activity and selectivity.



Scheme 2A.9: Synthesis of Mn@PMO-IL and its application in the synthesis of DHPMs: a) H_2O , HCl , (2M), P123, 40°C , 24h; b) Static conditions, 100°C ; c) Soxhlet extraction of surfactant

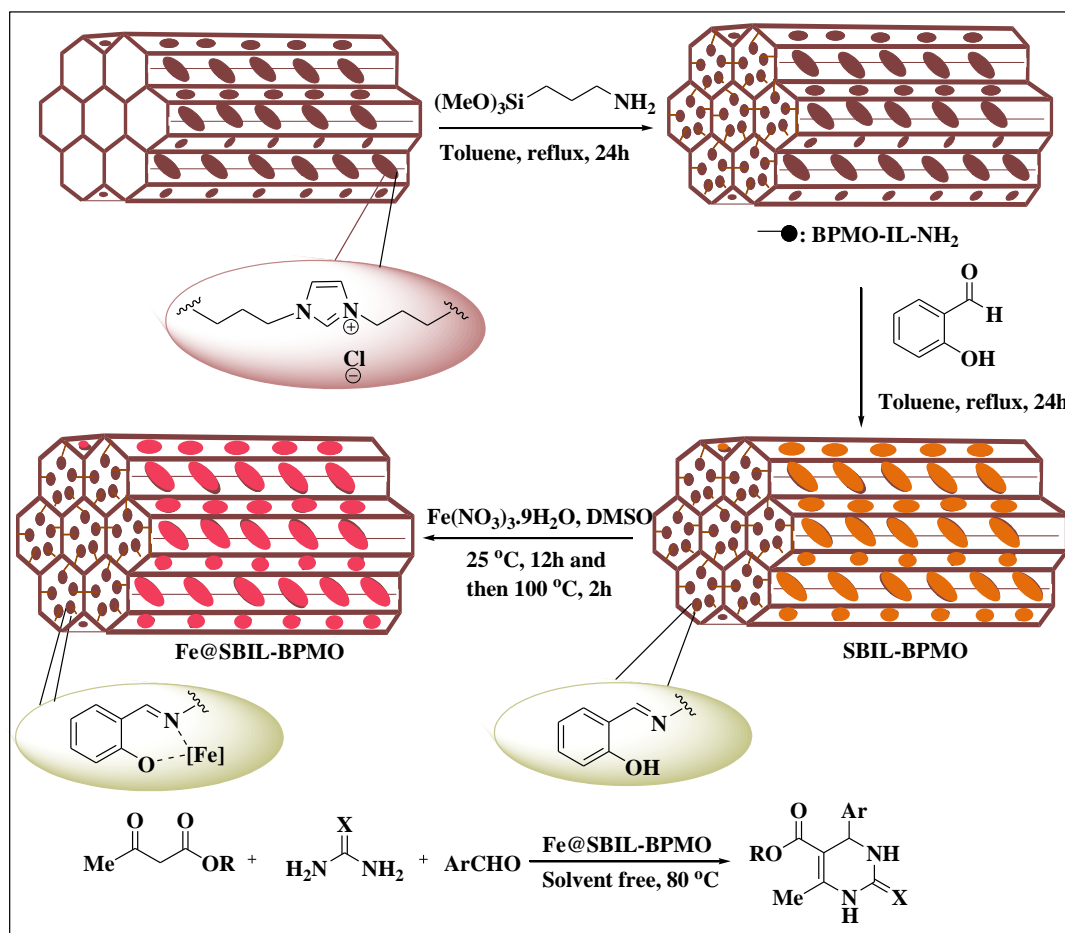
In the same year, Elhamifar et al. synthesized novel copper-loaded ionic liquid-based periodic mesoporous organosilica (Cu@PMO-IL) nanoparticles (**Scheme 2A.10**) [85] and characterized the mesoporous structure of the Cu@PMO-IL material via transmission electron microscopy (TEM) and nitrogen adsorption-desorption analysis. The authors confirmed the presence of copper species in the material framework X-ray photoelectron spectroscopy (XPS) and elemental analysis (EA). The catalytic application of the Cu@PMO-IL nanocatalyst was examined in the Biginelli condensation of different aldehydes with urea and alkylacetoacetates under solvent-free conditions and at moderate temperature. Moreover, the stability, reactivity and reusability of the catalyst were found improved against the reaction conditions.



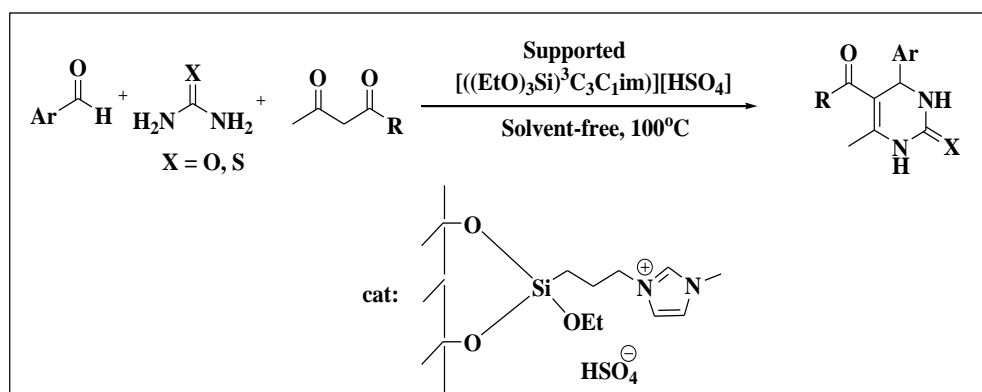
Scheme 2A.10: Synthesis of Cu@PMO-IL nanoparticles and their application in Biginelli reactions

Elhamifar and Nazari [86] in another study described the use of iron containing Schiff base and ionic liquid based bifunctional periodic mesoporous organosilica (Fe@SBIL-BPMO) (**Scheme 2A.11**) for the synthesis of 3, 4-dihydropyrimidinone/thione derivatives under solvent free reaction medium at $80\text{ }^\circ\text{C}$. The method showed high tolerance towards various aromatic electron withdrawing and electron donating group containing aldehydes. Aldehydes with electron donating substituents were converted to the desired products with high efficacy under the optimized reaction conditions. The synthesized nano-catalyst system showed high reactivity, durability as well as recyclability up to 15 consecutive cycles. TEM analysis of the recovered catalysts after fifth cycle confirmed the stability of the catalyst mesoporous framework.

Safari et al. [87] utilized acidic $[\text{((EtO)}_3\text{Si)}^3\text{C}_3\text{C}_1\text{im}][\text{HSO}_4]$ ionic liquid grafted on Fe_3O_4 magnetic nanoparticles as catalyst for the Biginelli synthesis of 3, 4-dihydropyrimidin-2(1H)-ones or -thiones (**Scheme 2A.12**) under solvent-free conditions at $100\text{ }^\circ\text{C}$ with 90–98% yields within 20–35 min. Different aromatic and heteroaromatic aldehydes were worked efficiently under the reaction conditions to form the corresponding products. The catalyst could be recovered easily from the reaction mixture by using a simple bar magnet and recycled up to 8th cycle with slight decrease in activity for the model reaction of benzaldehyde, ethyl acetoacetate, and urea.



Scheme 2A.11: Synthesis of the Fe@SBIL-BPMO catalyst and its application in the synthesis of 3, 4-dihydropyrimidinones/thiones



Scheme 2A.12: Synthesis of Biginelli 3,4-dihydropyrimidinones/thiones catalyzed by $[(\text{EtO})_3\text{Si})_3\text{C}_3\text{C}_1\text{im}][\text{HSO}_4]$ ionic liquid grafted on Fe_3O_4 magnetic nanoparticles

The literature review on various heterogenized ionic liquid systems highlights the progresses in this field over the years and encourages us to develop unique SILP systems using zeolite as the support. Also the review on use of different heterogeneous

ionic liquid systems in preparation of Biginelli 3, 4-dihydropyrimidinone derivatives signifies the superiority of these systems and uplifts the quest of researchers for such systems.

References

1. Breck, D. W. *Zeolite Molecular Sieves: Structure, Chemistry and Use*. John Wiley and Sons, London, page 4, 1974.
2. Smith, J. V. Origin and structure of zeolites. *Zeolite Chemistry and Catalysis*, 171:1-79, 1976.
3. Lutz, W. Zeolite Y: Synthesis, modification, and properties-a case revisited. *Advances in Materials Science and Engineering*, 2014:1-20, 2014.
4. Löwenstein, W. The distribution of aluminum in the tetrahedral of silicates and aluminates. *American Mineralogist*, 39:92-96, 1954.
5. Bhatia, S. *Zeolite Catalysis: Principles and Applications*. CRC Press, Inc., Boca Raton, Florida, 1990.
6. Baerlocher, Ch., Meier, W. M., and Holson, D. *Atlas of Zeolite Framework Types*. Elsevier, Amsterdam, 6th edition, 2001.
7. Bragg, W. L. *The Atomic Structure of Minerals*, Camell University press, Ithaca, New York, 1937.
8. Flanigen, E. M. In Rabo, J. A., editor; *Zeolite Chemistry and Catalysis*; volume 171 of *ACS Monograph Series*, page 80, American Chemical Society: Washington, DC, 1976.
9. Topsøe, N. Y., Pedersen, K., and Derouane, E. G. Infrared and temperature-programmed desorption study of the acidic properties of ZSM-5-type zeolites. *Journal of Catalysis*, 70(1):41-52, 1981.
10. Weitcamp, J. and Puppe, L. *Catalysis and Zeolites: Fundamentals and Applications*. Springer-Verlag Berlin Heidelberg, 1999
11. Hamid, S. B. A., Amin, M., and Ali, M. E. Zeolite supported ionic liquid catalyst for the synthesis of nano-cellulose from palm tree biomass. *Advanced Materials Research*, 925:52-56, 2014.
12. Jacobs, P. A., Flanigen, E. M., Jansen J.C., and Bekkum, H. v. *Introduction to Zeolite Science and Practice*, Elsevier Science Publishers B.V., Amsterdam, 2nd edition, 2001.

13. Beyer, H. K. Dealumination Techniques for Zeolites. In Karge, H. G. and Weitkamp, J., editors, *Molecular Sieves*, Vol. 3, pages 203-256, Springer-Verlag Berlin Heidelberg, 2002
14. Flanigan, E. M. Molecular sieve zeolite technology: the first twenty-five year. In *Proceedings of the 5th International Conference on Zeolites*, pages 760–780, Naples, Italy, 1980
15. Venuto P. B. and Habib Jr., E.T. Catalyst-feedstock-engineering interactions in fluid catalytic cracking. *Catalysis Reviews: Science and Engineering*, 18(1):1-150, 1978.
16. Rawlence, D. J. and Gosling, K. FCC catalyst performance evaluation. *Applied Catalysis*, 43(2):213–237, 1988.
17. Barrer, R. M. *Zeolites and Clay Minerals as Sorbents and Molecular Sieves*. Academic Press, London, UK, 1978.
18. Breck, D. W. “Crystalline zeolite Y.” U.S. Patent No. 3,130,007, issued April 21, 1964, Washington, DC: U.S. Patent and Trademark Office.
19. Rüscher, C. H., Salman, N., Buhl, J. C., and Lutz, W. Relation between growth-size and chemical composition of X and Y type zeolites. *Microporous and Mesoporous Materials*, 92(1):309-311, 2006.
20. Kerr, G. T. Chemistry of crystalline aluminosilicates. V. Preparation of aluminum-deficient faujasites. *The Journal of Physical Chemistry*, 72(7):2594-2596, 1968.
21. Beyer, H. K., Belenykaja, I. M., Hange, F., Tielen, M., Grobet, P. J., and Jacobs, P. A. Preparation of high-silica faujasites by treatment with silicon tetrachloride. *Journal of the Chemical Society, Faraday Transactions 1: Physical Chemistry in Condensed Phases*, 81(11):2889-2901, 1985.
22. McDaniel, C. W. and Maher, P. K. *Molecular Sieves. Society of Chemical Industry*, London, UK, page 186, 1968.
23. Ward, J. W. Thermal decomposition of ammonium Y zeolite. *Journal of Catalysis*, 27(1):157-161, 1972.
24. Lutz, W. Stabilizing effect of non-framework Al on the structure of dealuminated Y zeolites under hydrothermal conditions. *Crystal Research and Technology*, 25(8):921-926, 1990.

25. Ambs, W. J. and Flank, W. H. Thermal behavior of synthetic faujasite. *Journal of Catalysis*, 14(2):118-125, 1969.
26. Peri, J. B. The nature of ultrastable faujasite. In *Proceedings of the 5th International Congress on Catalysis*, Hightower, J.W. editor, pages 329–338, North-Holland, Miami Beach, Fla, USA, 1972.
27. Kerr, G. T., Chester, A. W., and Olson, D. H. Preparation of ultrahigh silicon faujasite by controlled-rate aluminium removal. In *Proceedings of the Symposium on Zeolites*, volume 24, pages 169-174, Jozsef Attila University, 1978, Acta Physica et Chemica, Nova Series.
28. Steel, A. T. and Dooryhee, E. Time dependence of the structural changes occurring in NH₄-Y zeolite on dealumination: a preliminary study using energy-dispersive X-ray diffraction. *Zeolites*, 13(5):336-340, 1993.
29. Li, S., Zheng, A., Su, Y., Zhang, H., Chen, L., Yang, J., Ye, C., and Deng, F. Brønsted/Lewis acid synergy in dealuminated HY zeolite: a combined solid-state NMR and theoretical calculation study. *Journal of the American Chemical Society*, 129(36):11161-11171, 2007.
30. Remy, M. J., Stanica, D., Poncelet, G., Feijen, E. J. P., Grobet, P. J., Martens, J. A., and Jacobs. P. A. Dealuminated H-Y zeolites: relation between physicochemical properties and catalytic activity in heptane and decane isomerization. *The Journal of Physical Chemistry*, 100(30):12440-12447, 1996.
31. Biaglow, A. I., Parrillo, D. J., Kokotailo, G. T., and Gorte, R. J. A study of dealuminated faujasites. *Journal of Catalysis*, 148(1):213-223, 1994.
32. Mirodatos, C. and Barthomeuf, D. Superacid sites in zeolites. *Journal of the Chemical Society, Chemical Communications*, 2:39-40, 1981.
33. Wang, Q. L., Giannetto, G., and Guisnet, M. Dealumination of zeolites III. Effect of extra-framework aluminum species on the activity, selectivity, and stability of Y zeolites in n-heptane cracking. *Journal of Catalysis*, 130(2):471-482, 1991.
34. Lónyi, F. and Lunsford, J. H. The development of strong acidity in hexafluorosilicate-modified Y-type zeolites. *Journal of Catalysis*, 136(2):566-577, 1992.
35. Riisager, A., Fehrmann, R., Haumann, M., and Wasserscheid, P. Supported ionic liquid phase (SILP) catalysis: an innovative concept for homogeneous catalysis

- in continuous fixed-bed reactors. *European Journal of Inorganic Chemistry*, 2006(4):695-706, 2006.
36. Pârvulescu, V. I. and Hardacre, C. Catalysis in ionic liquids. *Chemical Reviews*, 107(6):2615-2665, 2007.
37. DeCastro, C., Sauvage, E., Valkenberg, M. H., and Hölderich, W. F. Immobilised ionic liquids as Lewis acid catalysts for the alkylation of aromatic compounds with dodecene. *Journal of Catalysis*, 196(1):86-94, 2000.
38. Valkenberg, M. H. and Hölderich, W. F. Immobilisation of ionic liquids on solid supports. *Green Chemistry*, 4(2):88-93, 2002.
39. Pietschmann, B., Wei, M. A., Selvam, T., and SEXTL, G. Zeolite and Related Materials, Trends, Targets and Challenges. *In Proceedings of 4th FEZA Conference*, page 325, Paris, 2008.
40. Valkenberg, M. H., deCastro C., and Hölderich, W.F. 29-O-03-Novel Lewis-acid catalysts (NLACs): their properties, characterization and use in catalysis. *Studies in Surface Science and Catalysis*, 135:179, 2001.
41. Valkenberg, M. H., deCastro C., and Hölderich, W.F. Supported catalysts and their applications, *In Proceedings of the 4th International Symposium on Supported Reagents and Catalysts in Chemistry*, page 242, The Royal Society of Chemistry, Cambridge, 2001.
42. Jin, M. J., Taher, A., Kang, H. J., Choi, M., and Ryoo, R. Palladium acetate immobilized in a hierarchical MFI zeolite-supported ionic liquid: a highly active and recyclable catalyst for Suzuki reaction in water. *Green Chemistry*, 11(3):309-313, 2009.
43. Ntais, S., Moschovi, A., Dracopoulos, V., and Nikolakis, V. Ionic liquid/zeolite composites: synthesis and characterization using vibrational spectroscopy techniques. *ECS Transactions*, 33(7):41-47, 2010.
44. Ntais, S., Moschovi, A. M., Paloukis, F., Neophytides, S., Burganos, V. N., Dracopoulos, V., and Nikolakis, V. Preparation and ion transport properties of NaY zeolite-ionic liquid composites. *Journal of Power Sources*, 196(4):2202-2210, 2011.
45. Eguizábal, A., Lemus, J., Urbiztondo, M., Moschovi, A. M., Ntais, S., Soler, J., and Pina, M. P. Ammonium based ionic liquids immobilized in large pore

- zeolites: Encapsulation procedures and proton conduction performance. *Journal of Power Sources*, 196(9):4314-4323, 2011.
46. Arya, K., Rawat, D. S., and Sasai, H. Zeolite supported Brønsted-acid ionic liquids: an eco-approach for synthesis of spiro [indole-pyrido [3, 2-e] thiazine] in water under ultrasonication. *Green Chemistry*, 14(7):1956-1963, 2012.
47. Arya, K. and Prabhakar, B. Ionic liquid confined zeolite system: an approach towards water mediated room temperature synthesis of spiro [pyrazolo [3, 4-e] benzothiazepines]. *Green Chemistry*, 15(10):2885-2894, 2013.
48. Prabhakar, B., Kapil, A., Ravichandran, G., Kuvettu, M. P., Choudhury, S. P., Krishnan, V., Ray, S. K., Christopher, J., and Makhija, S. U.S. Patent No. 7,968,079. Washington, DC: U.S. Patent and Trademark Office, 2011.
49. Noroozifar, M., Khorasani-Motlagh, M., Parizi, M. B., and Akbari, R. Highly sensitive electrochemical detection of dopamine and uric acid on a novel carbon nanotube-modified ionic liquid-nanozeolite paste electrode. *Ionics*, 19(9):1317-1327, 2013.
50. Martínez Blanes, J. M., Szyja, B. M., Romero-Sarria, F., Centeno, M. Á., Hensen, E. J., Odriozola, J. A., and Ivanova, S. Multiple zeolite structures from one ionic liquid template. *Chemistry-A European Journal*, 19(6):2122-2130, 2013.
51. Yu, Y., Mai, J., Wang, L., Li, X., Jiang, Z., and Wang, F. Ship-in-a-bottle synthesis of amine-functionalized ionic liquids in NaY zeolite for CO₂ capture. *Scientific Reports*, 4(5997):1-8, 2014.
52. Li, Z. M., Zhou, Y., Tao, D. J., Huang, W., Chen, X. S., and Yang, Z. MOR zeolite supported Brønsted acidic ionic liquid: an efficient and recyclable heterogeneous catalyst for ketalization. *RSC Advances*, 4(24):12160-12167, 2014.
53. Losch, P., Pascual, A. M., Boltz, M., Ivanova, S., Louis, B., Montilla, F., and Odriozola, J. A. Ionic liquid immobilization on carbon nanofibers and zeolites: Catalyst design for the liquid-phase toluene chlorination. *Comptes Rendus Chimie*, 18(3):324-329, 2015.
54. Nagarajaiah, H., Mukhopadhyay, A., and Moorthy, J. N. Biginelli reaction: an overview. *Tetrahedron Letters*, 57(47):5135-5149, 2016.

55. De Souza, R. O., da Penha, E. T., Milagre, H., Garden, S. J., Esteves, P. M., Eberlin, M. N., and Antunes, O. A. The three-component Biginelli reaction: a combined experimental and theoretical mechanistic investigation. *Chemistry-A European Journal*, 15(38):9799-9804, 2009.
56. Ramos, L.M., Ponce de Leon y Tobio, A.Y., dos Santos, M.R., de Oliveira, H.C., Gomes, A.F., Gozzo, F.C., de Oliveira, A.L., and Neto, B.A. Mechanistic studies on lewis acid catalyzed biginelli reactions in ionic liquids: Evidence for the reactive intermediates and the role of the reagents. *The Journal of Organic Chemistry*, 77(22):10184-10193, 2012.
57. Puripat, M., Ramozzi, R., Hatanaka, M., Parasuk, W., Parasuk, V., and Morokuma, K. The Biginelli reaction is a urea-catalyzed organocatalytic multicomponent reaction. *The Journal of Organic Chemistry*, 80(14):6959-6967, 2015.
58. Sandhu, J. S. and Sandhu, S. S. Past, present and future of the Biginelli reaction: a critical perspective. *ARKIVOC: Online Journal of Organic Chemistry*, 1:66-103, 2012.
59. Wang, A., Liu, X., Su, Z., and Jing, H. New magnetic nanocomposites of ZrO_2 - Al_2O_3 - Fe_3O_4 as green solid acid catalysts in organic reactions. *Catalysis Science & Technology*, 4(1):71-80, 2014.
60. Zarnegar, Z. and Safari, J. Magnetic nanoparticles supported imidazolium-based ionic liquids as nanocatalyst in microwave-mediated solvent-free Biginelli reaction. *Journal of Nanoparticle Research*, 16(8):2509, 2014.
61. Khademinia, S., Behzad, M., Alemi, A., Dolatyari, M., and Sajjadi, S. M. Catalytic performance of bismuth pyromanganate nanocatalyst for Biginelli reactions. *RSC Advances*, 5(87):71109-71114, 2015.
62. Ghosh, B. K., Hazra, S., and Ghosh, N. N. Synthesis of Cu@ CF@ SBA15: A Versatile catalysts for (i) reduction of dyes, trifluralin, Synthesis of (ii) DHPMs by Biginelli reaction and (iii) 1, 2, 3-triazole derivatives by 'Click reaction'. *Catalysis Communications*, 80:44-48, 2016.
63. S Panda, S., Khanna, P., and Khanna, L. Biginelli reaction: a green perspective. *Current Organic Chemistry*, 16(4):507-520, 2012.
64. Brown, A.M., Kunze, D.L., and Yatani, A. The agonist effect of dihydropyridines on Ca channels. *Nature*, 311(5986):570-572, 1984.

65. Lloyd, J., Finlay, H.J., Atwal, K., Kover, A., Prol, J., Yan, L., Bhandaru, R., Vaccaro, W., Huynh, T., Huang, C.S., and Conder, M. Dihydropyrazolopyrimidines containing benzimidazoles as K V 1.5 potassium channel antagonists. *Bioorganic & Medicinal Chemistry Letters*, 19(18):5469-5473, 2009.
66. Patil, A. D., Kumar, N. V., Kokke, W. C., Bean, M. F., Freyer, A. J., Brosse, C. D., Mai, S., Truneh, A., and Carte, B. Novel alkaloids from the sponge *Batzella* sp.: inhibitors of HIV gp120-human CD4 binding. *The Journal of Organic Chemistry*, 60(5):1182-1188, 1995.
67. Kaan, H. Y. K., Ulaganathan, V., Rath, O., Prokopcová, H., Dallinger, D., Kappe, C. O., and Kozielski, F. Structural basis for inhibition of Eg5 by dihydropyrimidines: stereoselectivity of antimitotic inhibitors enastron, dimethylenastron and fluorastrol. *Journal of Medicinal Chemistry*, 53(15):5676-5683, 2010.
68. Lewis, R. W., Mabry, J., Polisar, J. G., Eagen, K. P., Ganem, B., and Hess, G. P. Dihydropyrimidinone positive modulation of δ -subunit-containing γ -aminobutyric acid type A receptors, including an epilepsy-linked mutant variant. *Biochemistry*, 49(23):4841-4851, 2010.
69. Chiang, A. N., Valderramos, J. C., Balachandran, R., Chovatiya, R. J., Mead, B. P., Schneider, C., Bell, S. L., Klein, M. G., Huryn, D. M., Chen, X. S., and Day, B. W. Select pyrimidinones inhibit the propagation of the malarial parasite, *Plasmodium falciparum*. *Bioorganic & Medicinal Chemistry*, 17(4):1527-1533, 2009.
70. Rajanarendar, E., Reddy, M. N., Murthy, K. R., Reddy, K. G., Raju, S., Srinivas, M., Praveen, B., and Rao, M. S. Synthesis, antimicrobial, and mosquito larvicidal activity of 1-aryl-4-methyl-3, 6-bis-(5-methylisoxazol-3-yl)-2-thioxo-2, 3, 6, 10b-tetrahydro-1H-pyrimido [5, 4-c] quinolin-5-ones. *Bioorganic & Medicinal Chemistry Letters* 20(20):6052-6055, 2010.
71. Mokale, S. N., Shinde, S. S., Elgire, R. D., Sangshetti, J. N., and Shinde, D. B. Synthesis and anti-inflammatory activity of some 3-(4, 6-disubstituted-2-thioxo-1, 2, 3, 4-tetrahydropyrimidin-5-yl) propanoic acid derivatives. *Bioorganic & Medicinal Chemistry Letters*, 20(15):4424-4426, 2010.

72. Virsodia, V., Pissurlenkar, R. R., Manvar, D., Dholakia, C., Adlakha, P., Shah, A., and Coutinho, E. C. Synthesis, screening for antitubercular activity and 3D-QSAR studies of substituted N-phenyl-6-methyl-2-oxo-4-phenyl-1, 2, 3, 4-tetrahydro-pyrimidine-5-carboxamides. *European Journal of Medicinal Chemistry*, 43(10):2103-2115, 2008.
73. Kidwai, M., Saxena, S., Khan, M. K. R., and Thukral, S. S. Synthesis of 4-aryl-7, 7-dimethyl-1, 2, 3, 4, 5, 6, 7, 8-octahydroquinazoline-2-one/thione-5-one derivatives and evaluation as antibacterials. *European Journal of Medicinal Chemistry*, 40(8):816-819, 2005.
74. Stefani, H. A., Oliveira, C. B., Almeida, R. B., Pereira, C. M. P., Braga, R. C., Cella, R., Borges, V. C., Savegnago, L., and Nogueira, C. W. Dihydropyrimidin-(2H)-ones obtained by ultrasound irradiation: a new class of potential antioxidant agents. *European Journal of Medicinal Chemistry*, 41(4):513-518, 2006.
75. Singh, B. K., Mishra, M., Saxena, N., Yadav, G. P., Maulik, P. R., Sahoo, M. K., Gaur, R. L., Murthy, P. K., and Tripathi, R. P. Synthesis of 2-sulfanyl-6-methyl-1, 4-dihydropyrimidines as a new class of antifilarial agents. *European Journal of Medicinal Chemistry*, 43(12):2717-2723, 2008.
76. Barrow, J. C., Nantermet, P. G., Selnick, H. G., Glass, K. L., Rittle, K. E., Gilbert, K. F., Steele, T. G., Homnick, C. F., Freidinger, R. M., Ransom, R. W., and Kling, P. In vitro and in vivo evaluation of dihydropyrimidinone C-5 amides as potent and selective $\alpha 1A$ receptor antagonists for the treatment of benign prostatic hyperplasia. *Journal of Medicinal Chemistry*, 43(14):2703-2718, 2000.
77. Horovitz, Z. P. (Squibb, E. R. and Sons). Eur. Pat. Appl. EP 1990,400, 665; Chem. Abstr. 1991, 115, 64793.
78. Crosson, C. E., Potter, D. E., Ondetti, M. A. Floyd, D., and Aberg, G. (Houston Biotechnology Inc.; Squibb, E. R. and Sons). PCT Int. Appl. WO 1990, 06, 118; Chem. Abstr. 1991, 114, 157224w
79. Wang, Z. T., Wang, S. C., and Xu, L. W. Polymer-supported ionic-liquid-catalyzed synthesis of 1, 2, 3, 4-tetrahydro-2-oxopyrimidine-5-carboxylates via Biginelli reaction. *Helvetica Chimica Acta*, 88(5):986-989, 2005.
80. Xu, L. W., Yang, M. S., Jiang, J. X., Qiu, H. Y., and Lai, G. Q. Ionic liquid-functionalized SBA-15 mesoporous material: efficient heterogeneous catalyst in

- versatile organic reactions. *Central European Journal of Chemistry*, 5(4):1073-1083, 2007.
81. Liu, Y., Peng, J., Zhai, S., Li, J., Mao, J., Li, M., Qiu, H., and Lai, G. Synthesis of ionic liquid functionalized SBA-15 mesoporous materials as heterogeneous catalyst toward Knoevenagel condensation under solvent-free conditions. *European Journal of Inorganic Chemistry*, 2006(15):2947-2949, 2006.
82. Kang, L. Q., Jin, D. Y., and Cai, Y. Q. Silica-supported ionic liquid Si-[SbSipim][PF₆]: an efficient catalyst for the synthesis of 3, 4-dihydropyrimidine-2-(1H)-ones. *Synthetic Communications*, 43(14):1896-1901, 2013.
83. Kang, L. Q., Cai, Y. Q., Peng, Y. Q., Ying, X. L., and Song, G. H. Silica-supported sulfonic acid-functionalized ionic liquid coated with [bmim][PF₆] as a scavenger for the synthesis of amides. *Molecular Diversity*, 15(1):109-113, 2011.
84. Elhamifar, D. and Shábani, A. Manganese-containing periodic mesoporous organosilica with ionic-liquid framework (Mn@ PMO-IL): a powerful, durable, and reusable nanocatalyst for the Biginelli reaction. *Chemistry–A European Journal*, 20(11):3212-3217, 2014.
85. Elhamifar, D., Hosseinpour, F., Karimi, B., and Hajati, S. Ionic liquid-based ordered mesoporous organosilica-supported copper as a novel and efficient nanocatalyst for the one-pot synthesis of Biginelli products. *Microporous and Mesoporous Materials*, 204:269-275, 2015.
86. Elhamifar, D. and Nazari, E. Preparation of iron-containing Schiff base and ionic liquid based bifunctional periodic mesoporous organosilica and its application in the synthesis of 3, 4-dihydropyrimidinones. *ChemPlusChem*, 80(5):820-826, 2015.
87. Safari, J. and Zarnegar, Z. Brønsted acidic ionic liquid based magnetic nanoparticles: A new promoter for the Biginelli synthesis of 3, 4-dihydropyrimidin-2(1H)-ones/thiones. *New Journal of Chemistry*, 38:358-365, 2014.

Chapter 2B

A study on structural changes of 1, 3-disulfoimidazolium trifluoroacetate ionic liquid/NaY zeolite composites and their catalytic uses for three component synthesis of 3, 4-dihydropyrimidinones

Published with small modification

Gogoi, P., Dutta, A.K., and Borah, R. Studies on Structural Changes and Catalytic Activity of Y-zeolite Composites of 1, 3-disulfoimidazolium trifluoroacetate Ionic Liquid (IL) for Three Component Synthesis of 3, 4-dihydropyrimidinones. *Catalysis Letters*, 147(3):674-685. 2017.

2B.1. Results and discussion

In this work, we aimed to synthesize functionalized hybrid material of ionic liquids using NaY zeolite as suitable choice of support for its well organized pore channels, high surface area and thermal stability in addition to environment friendly nature [1]. For this purpose, six acidic composites of Y-zeolite with 1, 3-disulfoimidazolium trifluoroacetate [Dsim][CF₃COO] ionic liquid (IL) were prepared by mixing [Dsim][CF₃COO] ionic liquid with NaY zeolite powder in six different percentage ratios (weight/weight) expressed as 3%, 5%, 10%, 20%, 50% and 80% in methanol. The structural changes of modified framework of zeolite were analyzed by FT-IR, Power XRD, SEM-EDX, TEM, TGA and BET techniques. The acidity of each IL composite is determined from Hammett function and evaluated as heterogeneous catalyst for three-component preparation of Biginelli 3, 4-dihydropyrimidinones under solvent-free method at 60 °C as well as using mechano chemical energy under mild condition (Scheme 2B.1).

Powder XRD analysis

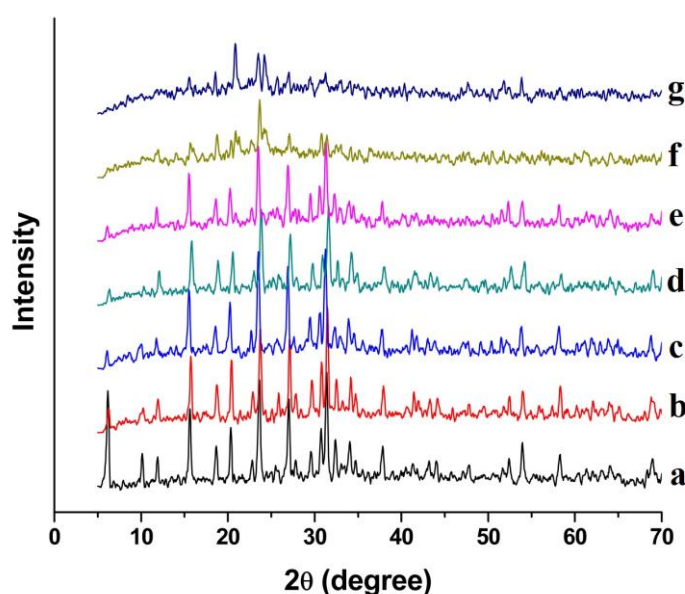
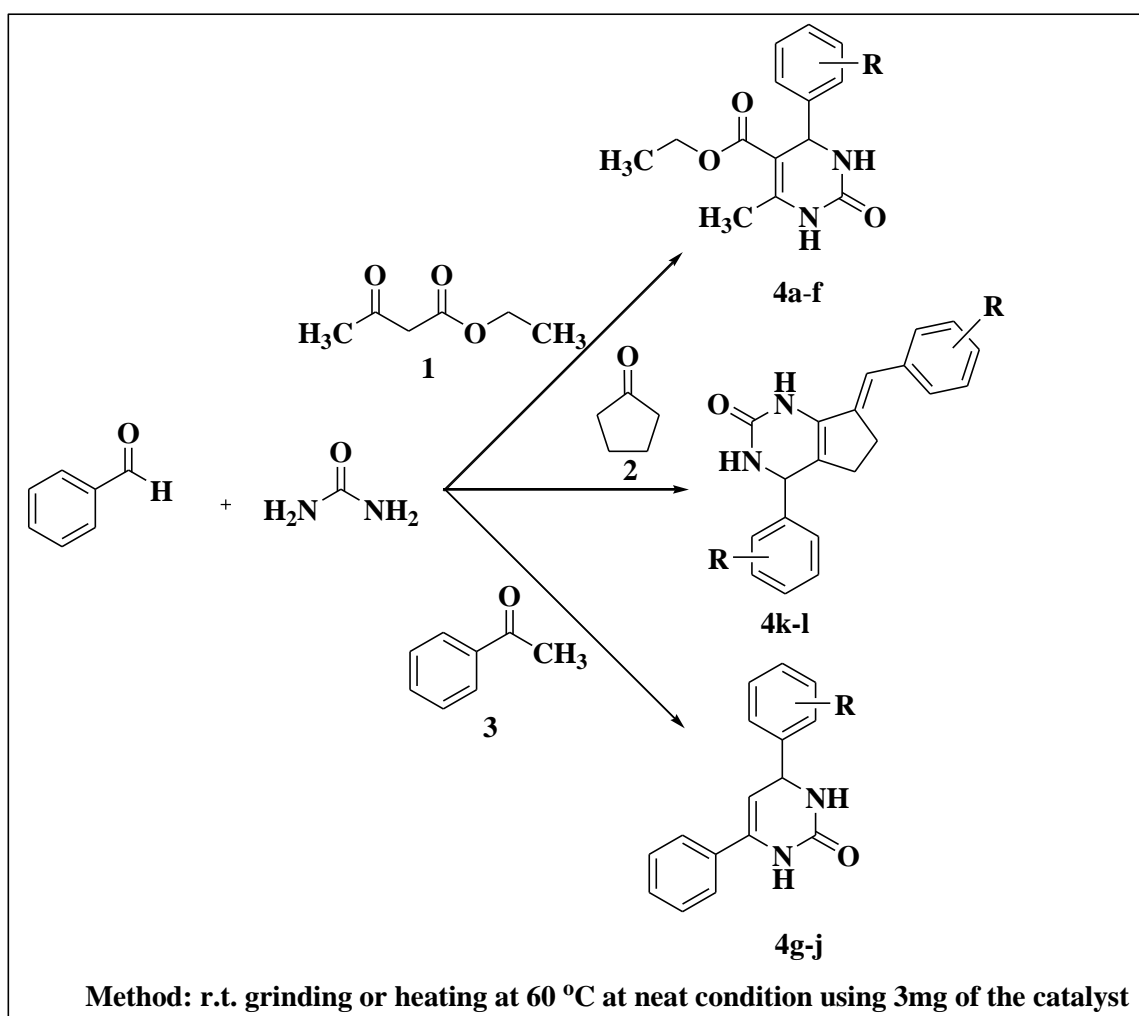


Fig. 2B.1: Powder XRD profile of the parent and the [Dsim][CF₃COO] encapsulated NaY zeolite samples: (a)NaY;(b)[Dsim][CF₃COO]/NaY=3%; (c)[Dsim][CF₃COO]/NaY=5%;(d)[Dsim][CF₃COO]/NaY=10%;(e)[Dsim][CF₃COO]/NaY=20%; (f)[Dsim][CF₃COO]/NaY=50%; (g)[Dsim][CF₃COO]/NaY=80%

In order to study the integrity of the NaY zeolite framework upon loading of [Dsim][CF₃COO] ionic liquid over it, we analyzed the parent and the IL encapsulated

samples via PXRD study. The PXRD profile for the parent zeolite (a) and six samples of the [Dsim][CF₃COO]/NaY composites with different loading of 3% (b), 5% (c), 10% (d), 20% (e), 50% (f) and 80% (g) respectively in ascending order is presented in **Fig. 2B.1**. The intensity of the basic peaks for NaY zeolite gradually decreases against increasing loading of the acidic IL [Dsim][CF₃COO] up to 20% (e). However, the composites retain the parent structure of the zeolite. The original structure of zeolite was destroyed in case of 50% (f) and 80% (g) composites. It might be due to acidic IL induced dealumination of Y-zeolite to some extra framework Al species in presence of higher amount of the ionic liquid.



Scheme 2B.1: Synthesis of 3, 4-dihydropyrimidinone derivatives

Partial dealumination converted a small portion of the crystalline zeolite structure into amorphous state with significant retention of the crystallinity up to the 20% loading (e). It is clearly reflected in **Fig. 2B.2**, which is generated by comparison of percent crystallinity of modified samples with the parent zeolite. The relative

crystallinity differences for four different composites (**b**, **c**, **d**, **e**) and the parent zeolite (**a**) were calculated by taking four high intensity peaks at $2\theta=15.54$, 23.54° , 26.90° & 31.28° using Equation-1 as follows :

$$\% \text{ Crystallinity} = (AS \times 100) / AR \text{-----(1)}$$

where AR is integrated area of the reference material under the peaks between a set of 2θ limits, AS represents integrated area of the sample under the peaks between the same set of 2θ limits as that of the reference.

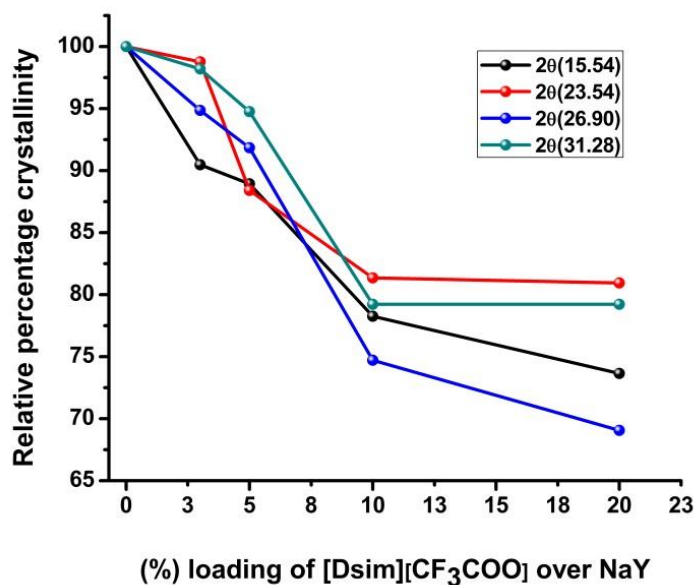


Fig. 2B.2: Comparison of the percent crystallinity of modified samples with the parent zeolite

FT-IR analysis

FT-IR spectra for the parent NaY zeolite and the six composites within the range $1800\text{-}400\text{ cm}^{-1}$ are presented in **Fig. 2B.3**. Up to 20% loading (**e**), IR spectra of the four composites showed slight shifting of fundamental absorption peaks of NaY zeolite with preservation of the basic framework. This observation confirmed that the loaded amount of $-\text{SO}_3\text{H}$ functionalized IL in the four composites (**b**, **c**, **d**, **e**) did not completely destruct the Y-zeolite framework via dealumination process. It suggests that the maximum permissible loading of the IL to be 20% over NaY zeolite surface. The peak at $1640\text{-}1638\text{ cm}^{-1}$ for all the composites can be assigned for bending vibration of water molecule attached to the zeolite structure which is overlapping with $-\text{C}=\text{N}-$ stretching vibration of imidazolium cation [2].

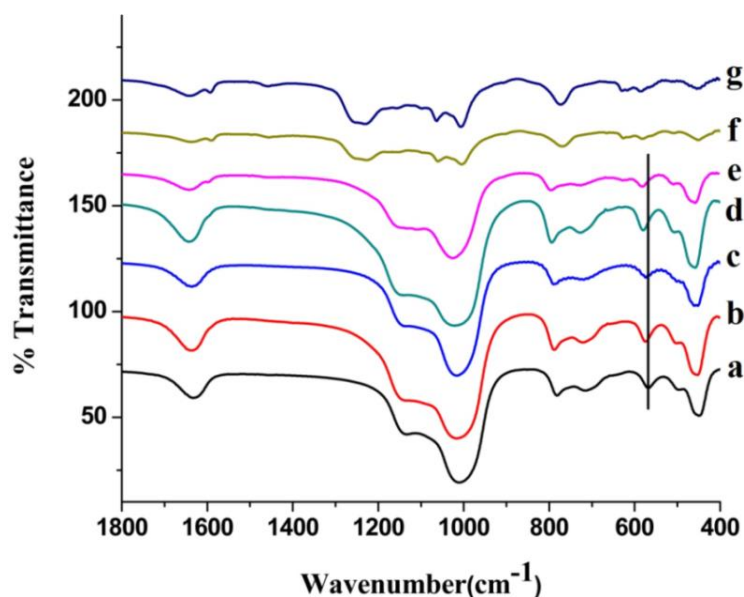


Fig. 2B.3: FT-IR profile of the parent and the [Dsim][CF₃COO] supported NaY zeolite samples: (a) NaY; (b)[Dsim][CF₃COO]/NaY=3%; (c)[Dsim]CF₃COO]/NaY=5%; (d)[Dsim]CF₃COO]/NaY=10%;(e)[Dsim][CF₃COO]/NaY=20%;(f)[Dsim]CF₃COO]/NaY=50%;(g) [Dsim]CF₃COO]/NaY=80%

The fundamental symmetric and asymmetric T-O (Si or Al) stretching vibrations of TO₄ unit of zeolite appeared at 796-784 cm⁻¹ and at 1026-1011 cm⁻¹ as weak to strong bands respectively for the composites (b), (c), (d) and (e). The asymmetric T-O (Si or Al) band becomes wider in case of 50% (f) and 80% (g) loaded composites. They showed another distinct band at 1246 cm⁻¹ by merging of S-O symmetric and asymmetric stretching vibration of -SO₃H groups at 1222 cm⁻¹ and 1075 cm⁻¹ [3]. The framework sensitive double-ring vibration peak of TO₄ unit at 568 cm⁻¹ shifted to around 572-584 cm⁻¹ for the (b), (c), (d) and (e) composites [4]. In case of highest loaded composites i.e. (f) and (g), we observed the appearance of a small hump at 628-632 cm⁻¹ for S-O bending vibration of -SO₃H group along with T-O-T bending vibration. These two composites witnessed the maximum dealuminated state in presence of highest amount of loaded acidic IL through collapsing of the basic double-ring vibration and bending vibration of TO₄ building block at 455-458 cm⁻¹ [5]. The substantial change of absorption patterns of highest loaded composites 50% (f) and 80% (g) revealed the existence of large number of extra framework Al species within these modified zeolite frameworks [5, 6].

From the double-ring vibration peak of various samples, we calculated the Si/Al ratio of different composites of [Dsim][CF₃COO]/NaY (**Table 2B.1**) using the empirical relation (Equation-2) as proposed by Rüscher et al. [7].

$$x = 3.857 - 0.00619 \nu_{\text{DR}}(\text{cm}^{-1}) \text{----- (2) where Si/Al} = (1-x)/x$$

The shifting of this band towards higher wave number in case of higher amount of ionic liquid loaded composites supports partial modification of the zeolite framework to some EFAI species.

Table 2B.1: Calculation of Si/Al ratio from IR spectra up to 20% loading composites

Sample name	$\nu_{\text{DR}} (\text{cm}^{-1})$	Si/Al ratio
NaY	568	1.93
[Dsim][CF ₃ COO]/NaY=3%	572	2.16
[Dsim][CF ₃ COO]/NaY=5%	572	2.16
[Dsim][CF ₃ COO]/NaY=10%	580	2.74
[Dsim][CF ₃ COO]/NaY=20%	584	3.13

The partial preservation of the zeolite framework at high temperature was evidenced from FT-IR spectra of the 20% (e) loaded composite at three different temperatures 250 °C, 350 °C and 450 °C as shown in **Fig. 2B.4**. The loss of some water molecules associated with the zeolite structure at high temperature could also be clearly appeared calcination from the gradual decrease of peak intensity of O-H bending vibration at 1643 cm⁻¹ of Y-zeolite (**Fig. 2B.5**)

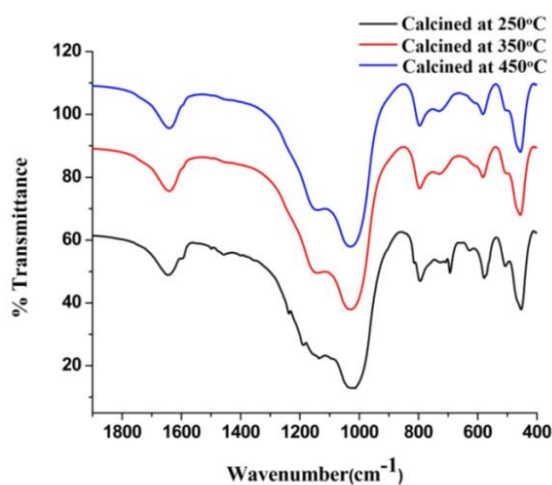


Fig. 2B.4: FT-IR spectra of the composite:[Dsim][CF₃COO]/NaY=20%(e) calcined at 250°C, 350 °C & 450 °C respectively

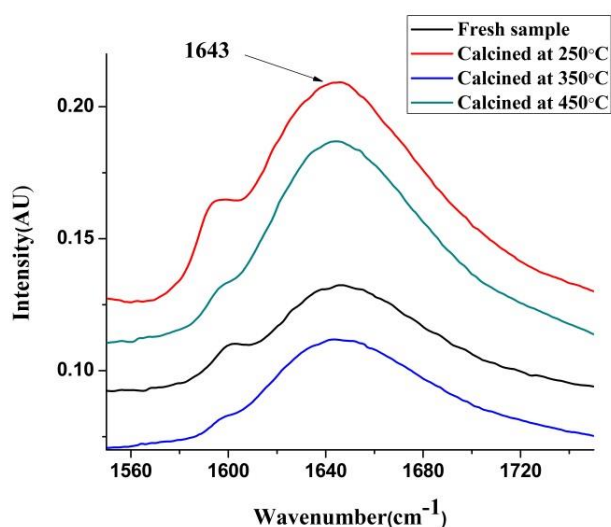


Fig. 2B.5: Comparison of intensity of O-H bending peak for calcined samples of (e) composite

From the FT-IR study, we can thus infer that during preparation of the composites the basic zeolite framework was modified to some extent with the formation of extra framework Al species up to the loading of 20% (e). Above that, extensive dealumination collapsed the basic structure of NaY in case of (f) and (g) which was reflected in the IR spectra in the **Fig. 2B.3**.

Thermogravimetric analysis

The comparative thermogravimetric analysis of the parent zeolite, the hybrid materials and the ionic liquid are presented in **Fig. 2B.6(A)** and **2B.6(B)**. In **Fig. 2B.6(A)**, the TGA profile of NaY(a), 3%(b), 5%(c) loaded samples shows approximate 18-20% weight loss around 100 °C without any further decomposition up to 600 °C which can be accounted for loss of only Na⁺ bound water or physisorbed water from the zeolite framework [8]. The amount of such water gradually reduces to 10-12% in case of 10% (d) and 20% (e) loaded composites as evident from TGA plot in the **Fig. 2B.6(B)**. Partial dealumination caused by -SO₃H moiety imparts a stabilizing effect in case of (d) and (e) composites by healing of Al defects with migrating H₄SiO₄ molecules [9]. On the other hand, both the curves of 50% (f) and 80% (g) loaded composites displayed 25% (approx.) weight loss in two steps below 150 °C followed by continuous weight loss up to 600 °C. These unusual observations represent a destabilized zeolite framework for these two composites in the highest dealuminated state caused by the acidic IL during preparation, which is also evident from the IR and PXRD studies. The most probable cause may be the loss of some water molecules from Al defects consisting of four

silanols (Si-OH) within the zeolite framework created during the dealumination process [10].

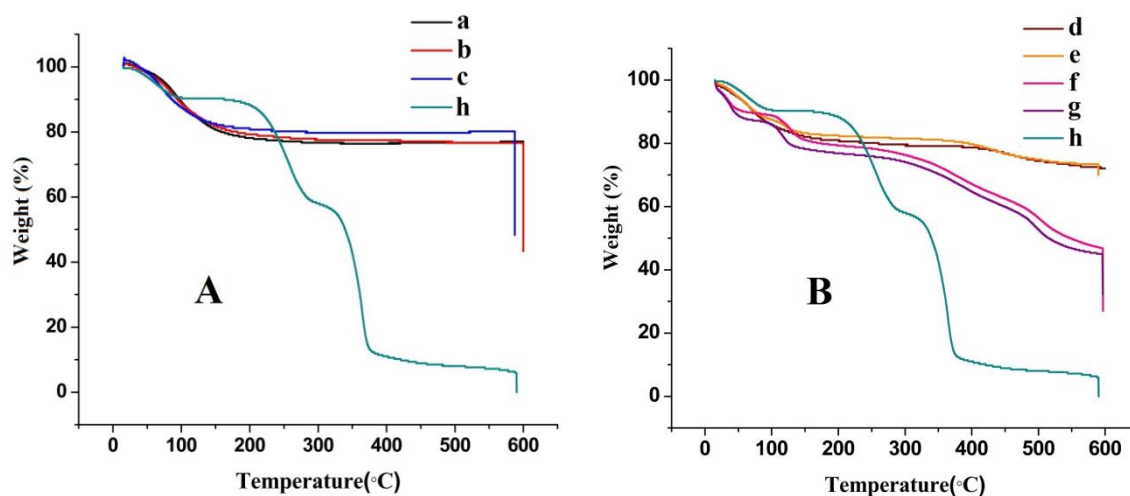
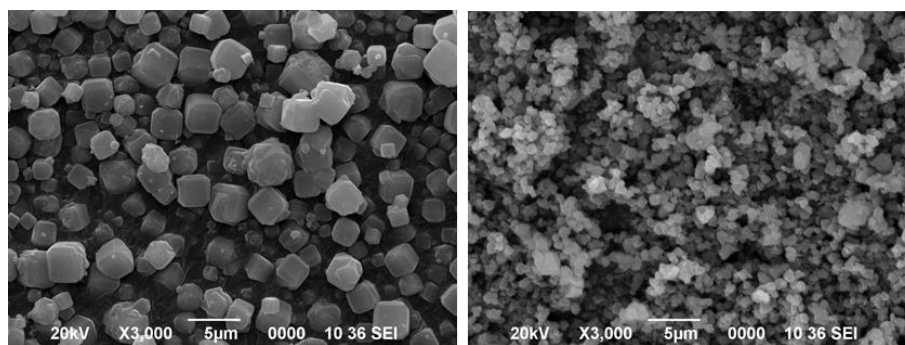


Fig. 2B.6(A) and 2B.6(B): TGA profiles of the parent and the [Dsim][CF₃COO] encapsulated NaY zeolite samples: (a)NaY;(b)[Dsim][CF₃COO]/NaY=3%; (c)[Dsim]CF₃COO/NaY=5%;(d)[Dsim]CF₃COO/NaY=10%;(e)[Dsim]CF₃COO/NaY=20%; (f)[Dsim]CF₃COO/NaY=50%; (g)[Dsim]CF₃COO/NaY=80%; (h) [Dsim]CF₃COO]

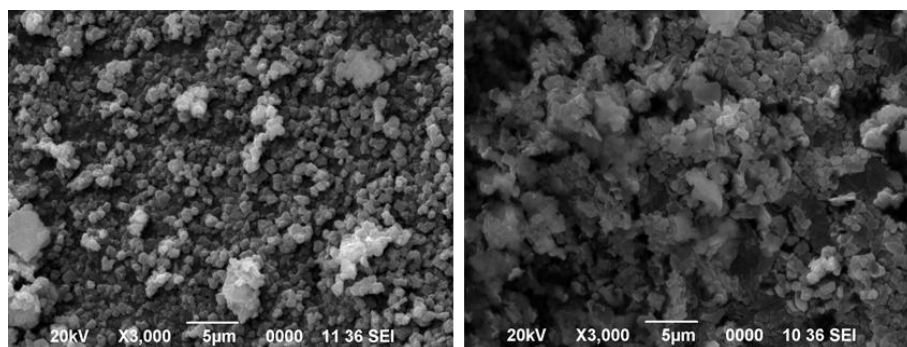
SEM-EDX analysis

The SEM images portrayed the surface of NaY zeolite to be consisting of perfectly cube shaped particles. As can be seen in **Fig. 2B.7**, the loaded IL particles form small clusters over the zeolite surface (composite **b** and **e**) which reduces the size and uniformity of the zeolite particles. The distribution of such clusters is observed to be more disordered for the 3% loaded composite. We found less clusters on the SEM image of 20% loaded composite with wide scattering of smaller crystallite size particles. The Y-zeolite structure got completely destroyed in case of highest loaded composite via dealumination of zeolite framework as observed from the IR study.



(i)

(ii)



(iii)

(iv)

Fig. 2B.7: SEM images of basic zeolite & composites: (i) NaY; (ii)[Dsim][CF₃COO]/NaY=3%;(iii)[Dsim]CF₃COO/NaY=20%;(iv)[Dsim]CF₃COO/NaY=80%

The EDX spectra of (e) composite showed the presence of constituent elements of [Dsim][CF₃COO] IL as well as NaY zeolite(**Fig. 2B.8**).

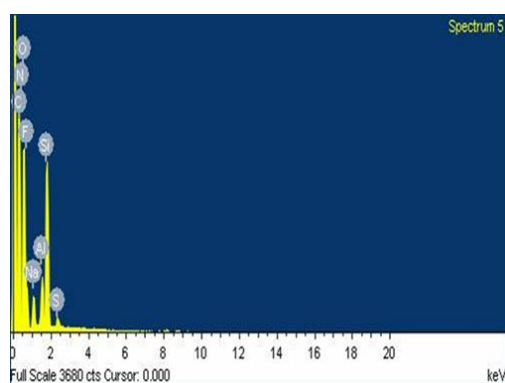
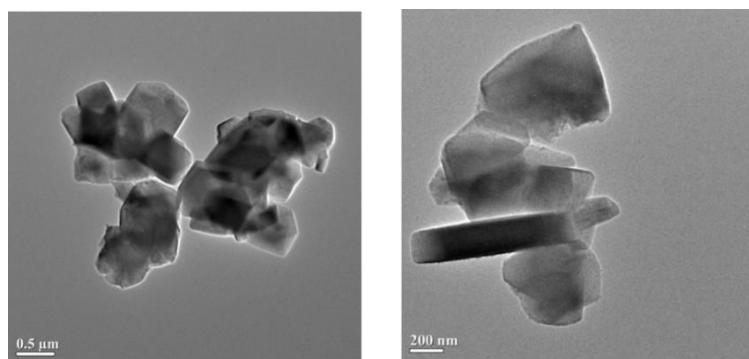


Fig. 2B.8: EDX spectra of [Dsim][CF₃COO]/NaY=20% (e)

TEM analysis



(a)

(b)

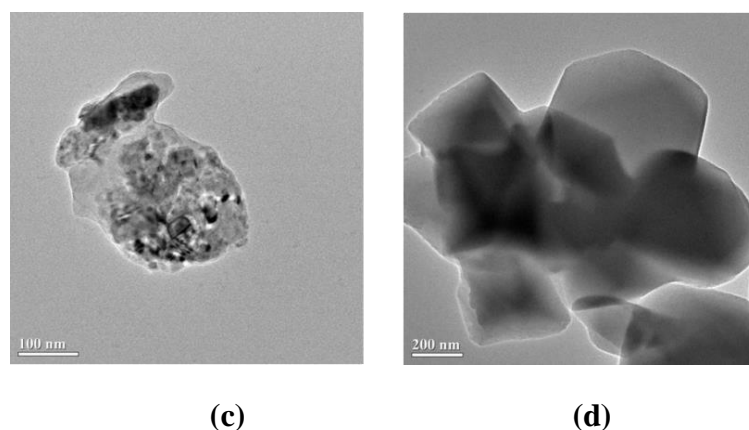


Fig. 2B.9: TEM images of 10% loaded composites

The TEM imaging in **Fig. 2B.9** was carried out for the 20% loaded composite. The TEM images displayed the encapsulation or accumulation of [Dsim][CF₃COO] on the external surface of zeolite pores with preservation of crystalline structure of Y-zeolite framework in this composite as confirmed from the PXRD pattern in the **Fig. 2B.1**.

BET analysis

The BET surface area measurement was performed for the 20% (**e**) loaded composite and NaY zeolite to check the change in porosity of the supported material. As evident from the **Table 2B.2**, the composite witnessed rapid loss in surface area and pore volume compared to the basic NaY zeolite as calculated from t-plot method (**Fig. 2B.10**) [11]. The abrupt decrease in surface area and micropore volume in case of the 20% (**e**) composite mainly refers to modification of zeolite framework into non-porous surface through encapsulation of acidic [Dsim][CF₃COO] which may reduce the access of zeolite pores for adsorption of N₂ gas.

Table 2B.2: Textural properties of NaY zeolite and the composite

Sample name	BET area (m ² /g) ^a	Micropore volume(cm ³ /g) ^b	Micropore area(m ² /g)	External surface area(m ² /g) ^b
NaY(a)	912.6	0.38	900.7	11.9
[Dsim][CF ₃ COO/NaY=20%(e)	291.0	0.15	287.4	3.6

^aMultipoint BET method; ^bt-plot method

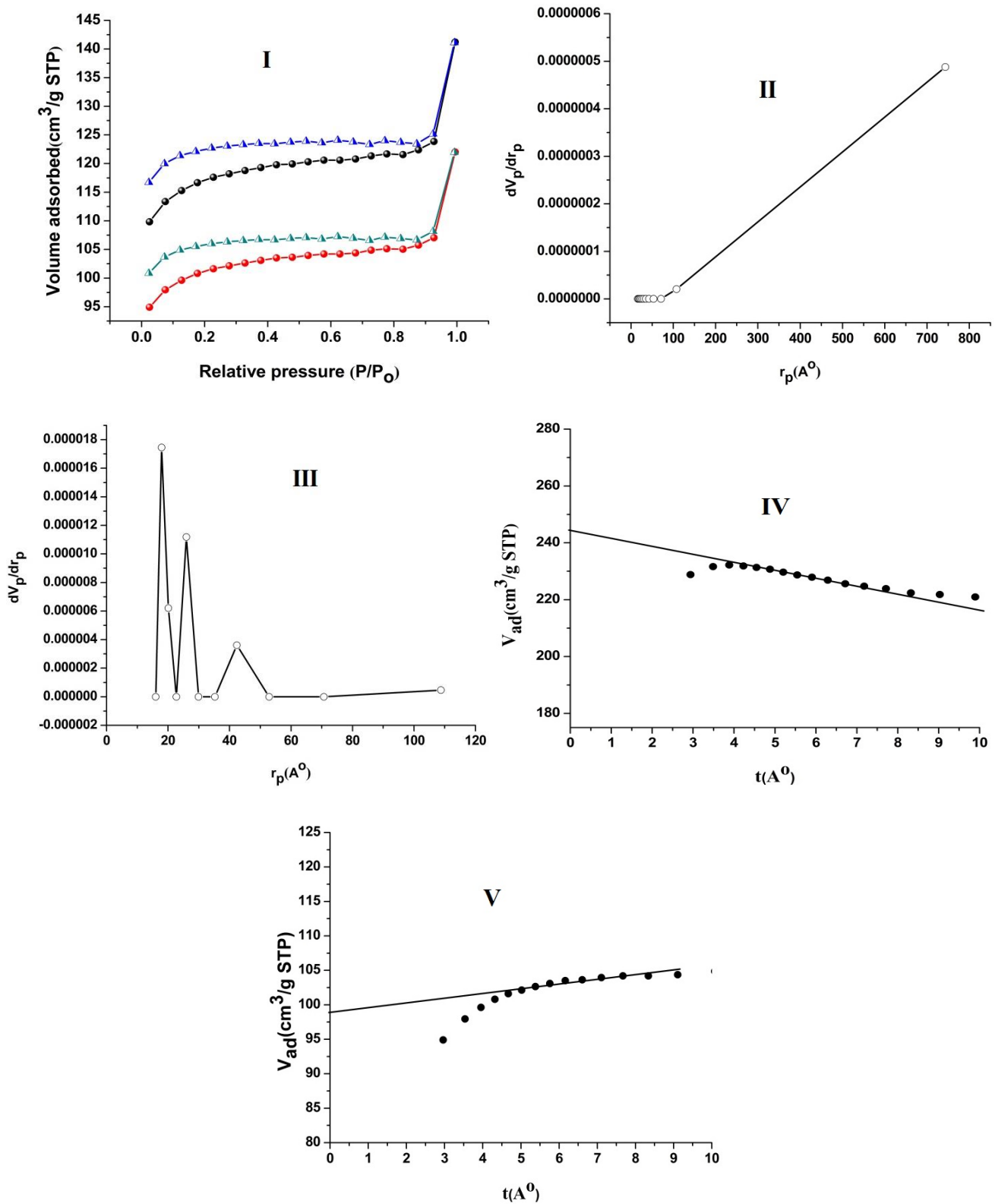


Fig. 2B.10: I: N₂ physisorption isotherms for NaY and composite (e); II: Pore size distribution plot for NaY; III: Pore size distribution plot for composite (e); IV: t-plot for NaY; V: t-plot for composite (e)

Acidity determination by Hammett plot

The Hammett acidity of four acidic composites up to 20% loading was determined from UV-Visible Hammett plot in **Fig.2B.11** according to the standard method as described in **Chapter 1C** using 4-nitroaniline as basic indicator in ethanol solution [12]. The procedure required the mixing of equal concentration of 4-nitroaniline (5 mg/L, $pK_a=0.99$) and catalyst (equal amounts of all) in ethanol solution. The Hammett functions H° of various composite materials are included in **Table 2B.3** to **Table 2B.5**.

Table 2B.3: Calculation of Hammett function from **Fig. 2B.11(A)**

Entry	Sample name ^a	A_{max}	[I]%	[IH]%	H°
1.	Blank	0.308	100	-	-
2.	[Dsim][CF ₃ COO]/NaY=3%	0.129	41.8	58.2	0.847
3.	[Dsim][CF ₃ COO]/NaY=5%	0.148	48.0	51.9	0.956
4.	[Dsim][CF ₃ COO]/NaY=10%	0.135	43.8	56.2	0.882
5.	[Dsim][CF ₃ COO]/NaY=20%	0.116	37.6	62.3	0.771

^aIndicator: 4-nitroaniline**Table 2B.4:** Calculation of the Hammett Function from **Fig. 2B.11(B)**

Entry	Sample name ^a	A_{max}	[I]%	[IH]%	H°
1.	Blank	0.308	100	-	-
2.	[Dsim][CF ₃ COO]/NaY=3%	0.096	31.17	68.83	0.646
3.	[Dsim][CF ₃ COO]/NaY=5%	0.110	35.71	64.29	0.735
4.	[Dsim][CF ₃ COO]/NaY=10%	0.078	25.32	74.68	0.520
5.	[Dsim][CF ₃ COO]/NaY=20%	0.051	16.79	83.21	0.295

^aIndicator: 4-nitroaniline**Table 2B.5:** Calculation of the Hammett Function from **Fig. 2B.11(C)**

Entry	Sample name ^a	A_{max}	[I]%	[IH]%	H°
1.	Blank	0.681	100	0	-
2.	[Dsim][CF ₃ COO]/NaY=3%	0.163	23.9	76.1	0.487
3.	[Dsim][CF ₃ COO]/NaY=5%	0.186	27.3	72.7	0.565
4.	[Dsim][CF ₃ COO]/NaY=10%	0.174	25.6	74.4	0.527

5.	[Dsim][CF ₃ COO]/NaY=20%	0.158	23.2	76.8	0.471
----	-------------------------------------	-------	------	------	-------

^aIndicator: 4-nitroaniline

The Hammett acidity for the composites can be expressed in decreasing order against their observed H^0 values as shown in **Table 2B.3** to **Table 2B.5**: [Dsim][CF₃COO]/NaY=20% (**e**) > [Dsim][CF₃COO]/NaY=3% (**b**) > [Dsim][CF₃COO]/NaY=10% (**d**) > [Dsim][CF₃COO]/NaY=5% (**c**). The higher acidity of 20% (**e**) loaded composite can be expected from gaining of extra stabilization through healing effects as mentioned in the TGA analysis (**Fig. 2B.6**) as well as lower rate of clustering of smaller size particle which is clearly visible in the SEM image (**Fig. 2B.7**). The unusual order of other three composites 3% (**b**), 5% (**c**) and 10% (**d**) can be accounted for different rate of clustering and their effects on blocking the active sites of composites for interaction with the basic indicator. The order of Hammett acidity did not change in **Fig. 2B.11(B)** and **Fig. 2B.11(C)** against the mixing of 1:4 and 2:3 ratio of the indicator and the respective four composite.

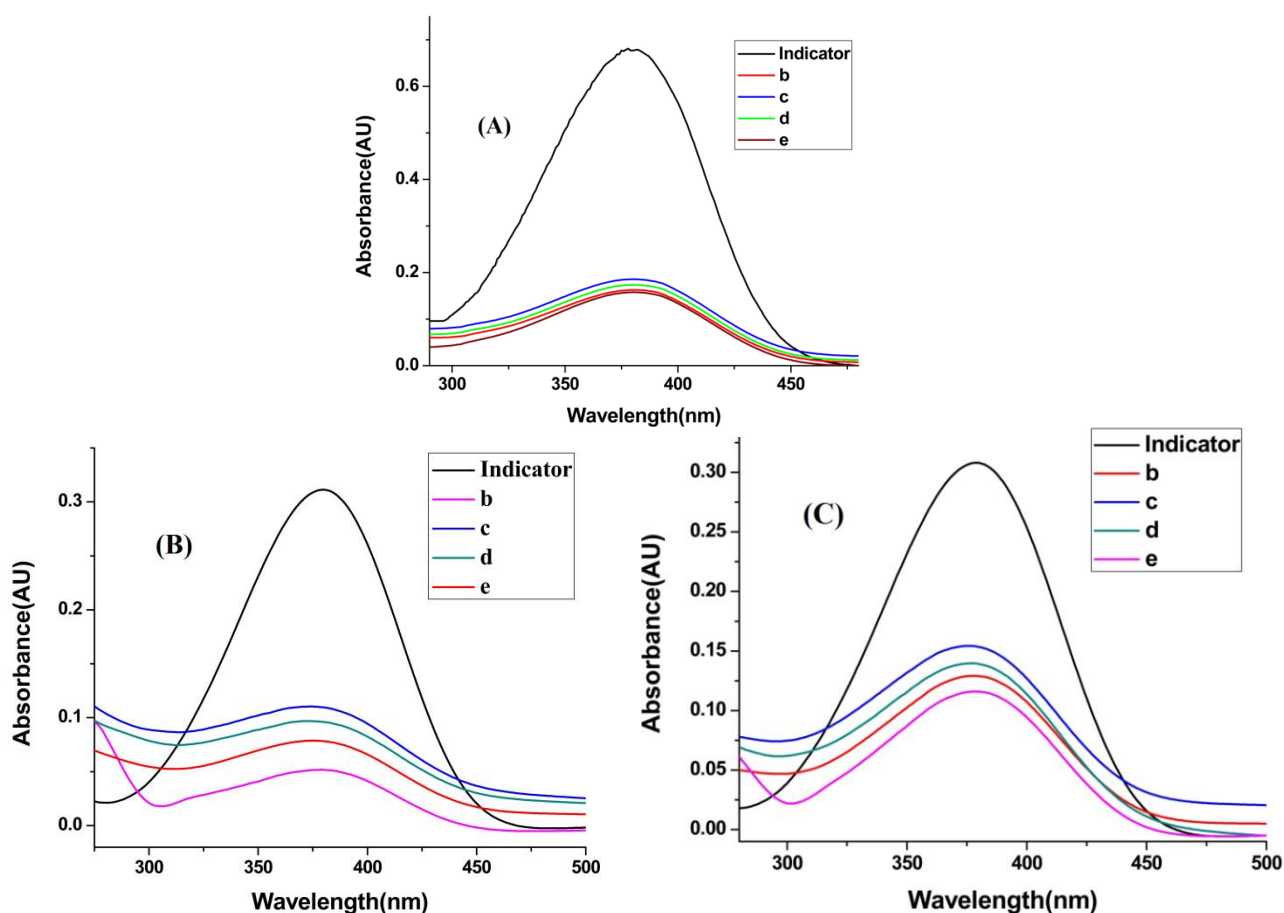


Fig.2B.11: Hammett plots of the composites: **b**: [Dsim][CF₃COO]/NaY=3%; **c**: [Dsim][CF₃COO]/NaY=5%; **d**: [Dsim][CF₃COO]/NaY=10%; **e**: [Dsim][CF₃COO]/NaY=20% in three conditions; (A) Hammett plot by mixing equal concentration of the

indicator and the composites; **(B)** Hammett plot by mixing 1:4 ratio of the indicator and the composites; **(C)** Hammett plot by mixing 2:3 ratio of the indicator and the composites

Evaluation of catalytic performance

To evaluate the activity of the catalysts under different conditions systematically, we choose the three component reaction of ethyl acetoacetate (1 mmol), benzaldehyde (1 mmol) and urea (1.5 mmol) as the model reaction under solvent free condition at different temperatures and the results are presented in **Table 2B.6**. Due to small difference in acidity of the synthesized catalysts as determined through the Hammett plots {**Fig.2B.11(A)**}, we tested the catalytic performance of four composites namely 3%**(b)**, 5%**(c)**, 10%**(d)** and 20%**(e)** with 10 mg under solvent-free method at 80 °C. Though there was small difference in the time required for completion of the reaction, the 20% loaded composite afforded the best result (entries 2-4). With the sole IL, it took 15 min to complete the reaction (entry 1). By reducing the amount of 20% loaded composite at 80 °C and 60 °C(entries 6-8), we observed excellent results in both cases (entry 7, 8) using 3 mg of the composite [Dsim][CF₃COO]/NaY=20% **(e)** for 2-10 min reaction.

Table 2B.6: Optimization of the reaction condition for the synthesis of model compound (**4a**)

Entry	Catalyst	Amount of the catalyst(mg)	Temp. (°C)	Time(min)	Product Yield ^a (4a) (%)
1	[Dsim][CF ₃ COO]	10	80	15	93
2	[Dsim][CF ₃ COO]/NaY=3%	10	80	4	94
3	[Dsim][CF ₃ COO]/NaY=5%	10	80	7	91
4	[Dsim][CF ₃ COO]/NaY=10%	10	80	5	92
5	[Dsim][CF ₃ COO]/NaY=20%	10	80	2	97
6	-do-	5	80	2	96
7	-do-	3	80	2	94
8	-do-	3	60	10	96
9	-do-	3	r.t.	15	95

			grinding		
--	--	--	----------	--	--

^aIsolated yields**Table 2B.7:** Substrate scope study for DHPMs derivatives using 20% loaded catalyst

Entry	β -ketoester/Ketone	Aldehyde	Time(min) (method)		Product yield (%) ^{a,b,c} (4a-l)	
			A	B	A	B
1.	CH ₃ COCH ₂ COOCH ₃	C ₆ H ₅ CHO	10	15	96	93
2.	-do-	4-NO ₂ C ₆ H ₄ CHO	15	18	94	92
3.	-do-	4-OCH ₃ C ₆ H ₄ CHO	20	24	92	90
4.	-do-	4-OHC ₆ H ₄ CHO	18	25	93	93
5.	-do-	4-ClC ₆ H ₄ CHO	30	30	94	91
6.	-do-	2,4-Cl ₂ C ₆ H ₃ CHO	35	35	92	90
7.	C ₆ H ₅ COCH ₃	C ₆ H ₅ CHO	15	30	94	89
8.	-do-	4-NO ₂ C ₆ H ₄ CHO	20	30	89	85
9.	-do-	4-CH ₃ OC ₆ H ₄ CHO	15	30	95	92
10.	-do-	1-Naphthaldehyde	28	35	85	82
11.	Cyclopentanone	C ₆ H ₅ CHO	25	32	92	87 ^d
12.	-do-	4-NO ₂ C ₆ H ₄ CHO	25	35	93	88

^aIsolated yields; ^bMethod A: Reactions were performed at 60 °C, Method B: Reactions were conducted using mortar and pestle under solvent-free grinding at ambient temperature; ^cMelting points of known compounds were compared with the literature values in supporting file [13-16]; ^dUsing 2 equivalent of aldehydes

For the sake of much milder condition to be developed, the reaction was carried out at room temperature using mechanical energy. It only took 15 mins to complete the reaction with an excellent yield of 93% (entry 9). Therefore, we extended our studies for the preparation of other derivatives of DHPMs through variation of aromatic aldehydes and keto compound in presence of 3 mg of 20% (**e**) loaded catalyst under solvent-free medium at 60 °C and at mild condition using grinding method. All these observations were included in **Table 2B.7**.

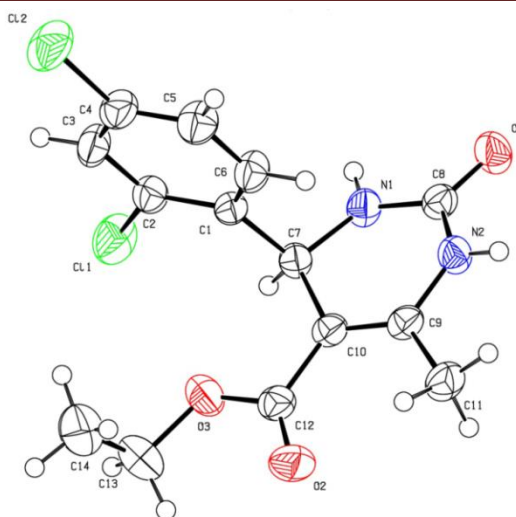


Fig. 2B.12: Single crystal X-ray analysis of **4f**

Single crystal X-ray analysis was performed for the 3, 4-dihydropyrimidine derivative **4f** (Table 2B.7, entry 6) which confirmed the presence of basic DHPM unit (Fig. 2B.12) [17].

Recyclability profile of the catalyst

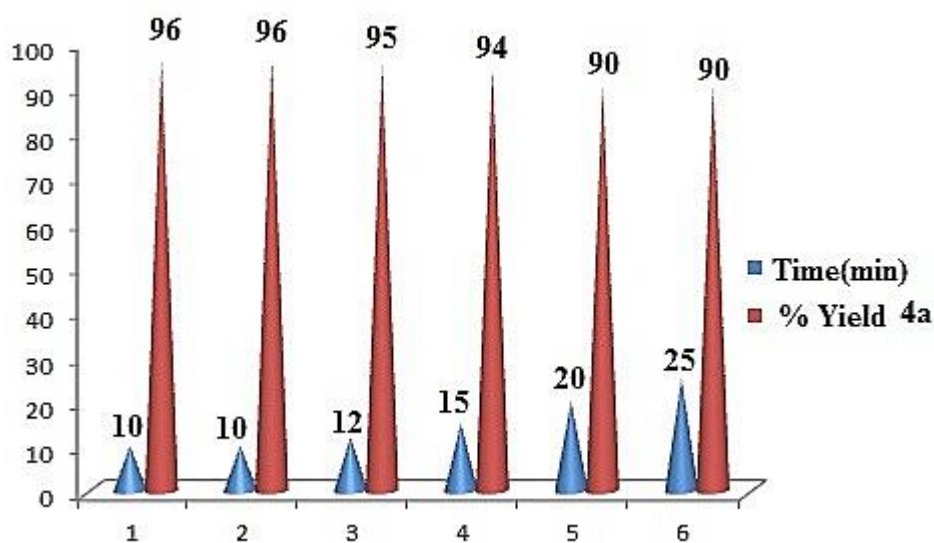


Fig. 2B.13: Recyclability profile for the composite: [Dsim][CF₃COO]/NaY=20% (e)

The recyclability profile of 20% loaded composite (e) was evaluated for the preparation of **4a** from the mixture of 3 mmol of β -keto ester and benzaldehyde with 4.5 mmol of urea under the optimized condition and it was found that the catalyst maintains very good activity up to 6th repetitive cycle (Fig. 2B.13). After the reaction was over, the catalyst surface was washed with cold water and hot EtOH and then it was dried in

oven 70 °C to make it ready for the next cycles of reactions. With increased number of cycles, the catalyst slowly lost its efficiency which was reflected in decreasing percentage yields of expected product with gradual rise of reaction time for completion of the reaction.

Characterization of the spent catalyst

The spent catalyst was again subjected for FT-IR analysis (**Fig. 2B.14**) after every alternate cycle to observe the effect of repeated thermal treatment and washing with hot ethanol on the ratio of Si/Al for dealumination which may slightly decrease the catalytic activity of spent catalyst in next consecutive cycles. **Table 2B.8** shows the retention of initial Si/Al ratio up to 4th cycle after which it indicates a higher value of Si/Al ratio due to formation of more extra framework Al species from 6th cycle onwards.

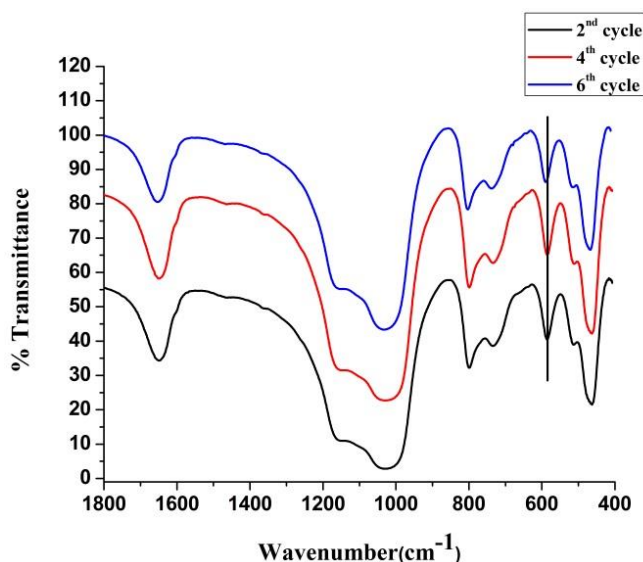


Fig. 2B.14: FT-IR spectra for the reused catalyst

Table 2B.8: Calculation of Si/Al ratio for the reused catalyst

Sample label	ν_{DR} (cm ⁻¹)	Si/Al ratio
Fresh	584	3.13
2 nd cycle residue	584	3.13
4 th cycle residue	584	3.13
6 th cycle residue	589	3.73

Likewise, the PXRD pattern of used catalyst (**Fig. 2B.15**) also displays reduction of peak intensity of the composite material after every alternate cycle which can be attributed for loss of crystallinity of spent catalyst.

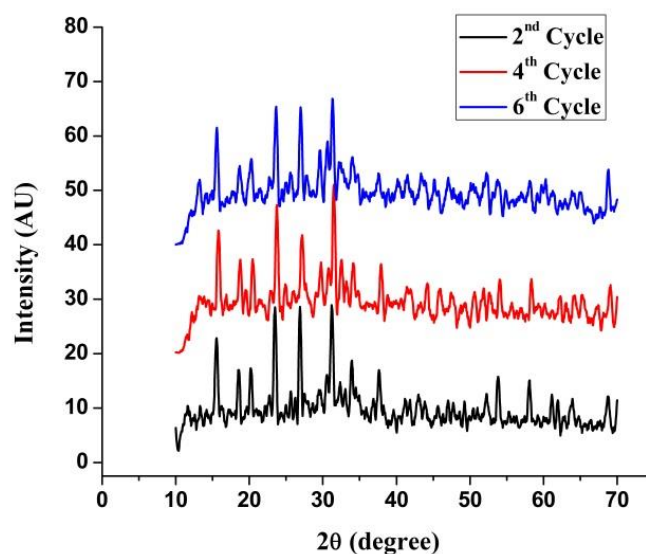


Fig. 2B.15: P-XRD diffraction pattern for used catalyst

2B.2. Conclusion

In this study, we analyzed the structural changes of parent NaY zeolite within the framework of modified composites [Dsim][CF₃COO]/NaY using different analytical techniques from which we identified 20% (e) loading as the best acidic composite from the Hammett function with thermal stability up to 450 °C. Loading above this percentage was harmful for the zeolite framework due to maximum dealumination as evidenced from the FT-IR and PXRD patterns of the 50% (f) and 80% (g) loaded composites. Formation of EFAl species on loading of the acidic IL affected the Si/Al ratio of the composites which in turn may also affect the acidity scale of the composites. The strong acidic composite 20% (e) was examined as heterogeneous catalyst for synthesis of DHPMs derivatives under solvent-free medium at 60 °C and at ambient temperature using solvent-free grinding method. The desired products were formed in excellent yields within short reaction times. The reusability study for composite e indicates its high catalytic activity up to 6th consecutive cycles. FT-IR and P-XRD analysis data for reused catalyst support the integrity of the system even after 6th cycle.

2B.3. Experimental Section

All the chemicals were purchased from different commercial suppliers in pure state. The composites were fully characterized via FT-IR, P-XRD, TGA, SEM-EDX, TEM, BET and UV-Vis techniques. The dealuminated state of the modified zeolite frameworks was confirmed via FT-IR and P-XRD studies. The synthesized products were identified by FT-IR, ^1H NMR, ^{13}C NMR, CHN analyses and also from their melting point. Single crystal data of compound **4f** was collected on a Bruker SMART APEX II CCD diffractometer.

General procedure for preparation of six composites of [Dsim][CF₃COO]/NaY:

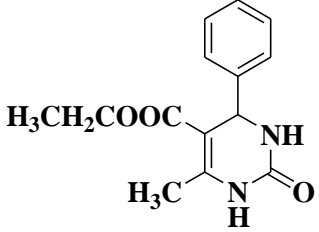
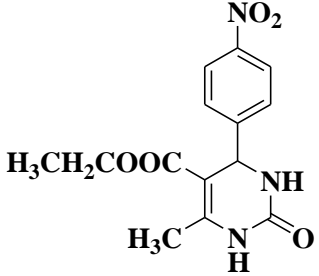
The synthesis of [Dsim][CF₃COO]/NaY composite involved in two steps. Initial step involved the synthesis of 1, 3-disulfoimidazolium trifluoroacetate [Dsim][CF₃COO] IL according to literature procedure [3]. Wet impregnation method was used to synthesize different composition of [Dsim][CF₃COO]/NaY composite. For this purpose, the following steps were practiced: (i) NaY zeolite were outgassed at 300 °C for 12 h, (ii) [Dsim][CF₃COO] ionic liquid and the zeolite powder were added in methanol in a 50 mL round bottom flask in six different percentage (weight/weight) ratios (namely 3%, 5%, 10%, 20%, 50% and 80%), (iii) the suspension was refluxed in methanol for overnight, (iv) the solvent was evaporated in rotary evaporator to get the hybrid acidic catalyst, (v) finally it was treated at 90 °C in vacuum oven for 3 hour to remove any traces of unwanted solvent molecule.

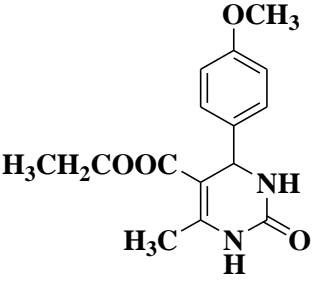
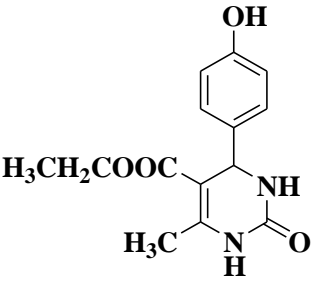
General method for the preparation of 3, 4-dihydropyrimidinones derivatives (4):

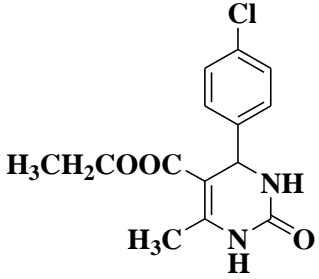
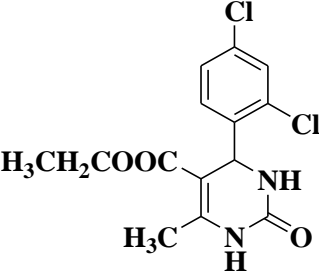
A mixture of aromatic aldehyde (1 mmol), ethyl acetoacetate/acetophenone/cyclopentanone (1 mmol) and urea (1.5 mmol) was treated at 60 °C under neat condition (or solvent-less grinding method using mortar and pestle at ambient temperature) utilizing 3 mg of 20% loaded [Dsim][CF₃COO]/NaY composite for the appropriate time until the reaction was complete. The progress of the reaction was monitored with thin layer chromatography in presence of EtOAc and petroleum ether (1:2) as mobile phase. The mixture was diluted with hot ethanol (3 mL) to dissolve the crude product. The catalyst was recovered as pure solid residue after filtration of ethanol solution and then washed three times with hot ethanol. The product was isolated as solid precipitate after

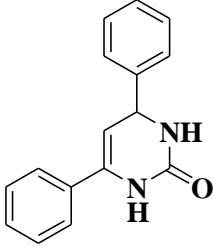
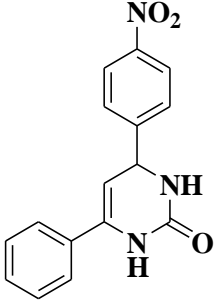
addition of water to the ethanol solution with vigorous stirring. Recrystallization of the crude product from saturated ethanol gave analytically pure product.

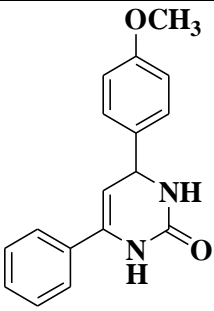
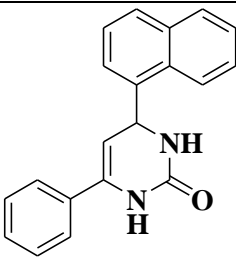
2B.4. Spectral data of the 3, 4-dihydropyrimidinone derivatives

Products	Spectral data
 <p>(Table 2B.7, entry 1)</p>	<p>5-Ethoxycarbonyl-6-methyl-4-phenyl-3,4-dihydropyrimidin-2(1H)-one 4a: White solid, M.P.(°C): 200-201(202-203) [13]; FT-IR(KBr): 3312, 1645, 1596, 1536, 1493, 1448, 1370, 1309, 1231, 1203, 1133, 1089, 1027, 917, 878, 749, 697 cm⁻¹; ¹H NMR (400 MHz, DMSO-d₆): δ 9.15 (s, 1H), 7.74 (s, 1H), 7.26-7.28 (m, 2H), 7.19-7.21 (m, 3H), 5.11 (d, <i>J</i> = 2.7 Hz, 1H), 3.93 (q, <i>J</i> = 7.3 Hz, 2H), 2.21 (s, 3H), 1.05 (t, <i>J</i> = 7.3 Hz, 3H); ¹³C NMR (100 MHz, DMSO-d₆): δ 165.9, 152.7, 148.9, 145.4, 128.9, 127.8, 126.8, 99.8, 59.7, 54.5, 18.3, 14.6; CHN analysis(%): C₁₄H₁₆N₂O₃: cal. C 64.6, H 6.30, N 10.68; found C 64.63, H 6.34, N 10.70.</p>
 <p>(Table 2B.7, entry 2)</p>	<p>5-Ethoxycarbonyl-6-methyl-4-(4-nitrophenyl)-3,4-dihydropyrimidin-2(1H)-one (4b): Off white solid M.P.(°C): 205-207(206-208) [13]; FT-IR(KBr): 3329, 1670, 1580, 1540, 1498, 1432, 1335, 1303, 1234, 1199, 1138, 1084, 1025, 928, 877, 752, 690 cm⁻¹; ¹H NMR (400 MHz, DMSO-d₆): δ 9.32 (s, 1H), 8.19 (d, <i>J</i> = 8.7 Hz, 2H), 7.86 (s, 1H), 7.45 (d, <i>J</i> = 8.7 Hz, 2H), 5.22 (s, 1H), 3.93 (q, <i>J</i> = 7.3 Hz, 2H), 2.22 (s, 3H), 1.05 (t, <i>J</i> = 6.9 Hz, 3H); ¹³C NMR (100 MHz, DMSO-d₆):</p>

	<p>δ165.5, 158.2, 152.5, 152.3, 147.2, 128.2, 127.8, 124.4, 123.8, 98.2, 59.9, 59.2, 54.2, 18.4, 14.6; CHN analysis(%): C₁₄H₁₅N₃O₅; cal. C 55.06, H 5.04, N 13.7; found C 55.10, H 5.08, N 13.82.</p>
 <p>(Table 2B.7, entry 3)</p>	<p>5-Ethoxycarbonyl-6-methyl-4-(4-methoxyphenyl)-3,4-dihydropyrimidin-2(1H)-one 4c: Off white Solid, M.P.(°C): 202-204(202-203) [13]; FT-IR(KBr): 3315, 1670, 1587, 1542, 1496, 1443, 1343, 1309, 1236, 1208, 1134, 1086, 1034, 913, 874, 745, 687 cm⁻¹; ¹H NMR (400 MHz, DMSO-d₆): δ 9.11 (s, 1H), 7.63 (s, 1H), 7.11 (d, <i>J</i> = 8.7 Hz, 2H), 6.82 (d, <i>J</i> = 8.7 Hz, 2H), 5.04 (s, 1H), 3.92 (q, <i>J</i> = 6.9 Hz, 2H), 3.67 (s, 3H), 2.19 (s, 3H), 1.05 (t, <i>J</i> = 7.4 Hz, 3H); ¹³C NMR (100 MHz, DMSO-d₆): δ 165.9, 158.9, 152.7, 148.6, 137.6, 127.9, 114.2, 100.0, 59.7, 55.6, 53.8, 18.3, 14.6; CHN analysis(%): C₁₅H₁₈N₂O₄; cal. C 62.86, H 6.84, N 9.55; found C 61.88, H 6.86, N 9.56.</p>
 <p>(Table 2B.7, entry 4)</p>	<p>5-Ethoxycarbonyl-6-methyl-4-(4-hydroxyphenyl)-3,4-dihydropyrimidin-2(1H)-one 4d: Yellow Solid, M.P.(°C): 225-227(224-226) [13]; FT-IR(KBr): 3265, 3124, 2978, 1724, 1704, 1656, 1476, 1456, 1432, 1396, 1290, 1222, 1089, 1012, 782, 684 cm⁻¹; ¹H NMR (400 MHz, DMSO-d₆): δ 9.36 (s, 1H), 9.05 (s, 1H), 7.57 (s, 1H), 6.99 (d, <i>J</i> = 8.7 Hz, 2H), 6.63 (d, <i>J</i> = 8.7 Hz, 2H), 5.0 (s, 1H), 3.91 (q, <i>J</i> = 7.3 Hz, 2H), 2.18 (s, 3H), 1.04 (t, <i>J</i></p>

	<p>= 7.3 Hz, 3H); ^{13}C NMR (100 MHz, DMSO-d_6): δ 165.9, 157, 152.7, 148.3, 135.9, 127.9, 115.5, 100.3, 59.7, 53.9, 18.3, 14.6.; CHN analysis(%): $\text{C}_{14}\text{H}_{16}\text{N}_2\text{O}_4$: cal. C 60.86, H 5.84, N 10.14, found C 60.84, H 5.90, N 10.12.</p>
<div style="text-align: center;">  <p>(Table 2B.7, entry 5)</p> </div>	<p>5-Ethoxycarbonyl-6-methyl-4-(4-chlorophenyl)-3,4-dihydropyrimidin-2(1H)-one 4e: Light pink Solid, M.P.(°C): 183-184(181-183) [13]; FT-IR(KBr): 3245, 3118, 2980, 1726, 1705, 1649, 1490, 1462, 1422, 1383, 1322, 1290, 1222, 1089, 1012, 782, 684, 459 cm^{-1}; ^1H NMR (400 MHz, DMSO-d_6): δ 9.25 (s, 1H), 7.73 (s, 1H), 7.36 (d, J = 8.3 Hz, 2H), 7.21 (d, J = 8.2 Hz, 2H), 5.14 (d, J = 3.2 Hz, 1H), 3.93 (q, J = 6.8 Hz, 2H), 2.20 (s, 3H), 1.05 (t, J = 7.3 Hz, 3H); ^{13}C NMR (100 MHz, DMSO-d_6): δ 165.7, 152.4, 149.3, 144.3, 132.3, 128.9, 128.7, 99.3, 59.8, 53.9, 18.3, 14.6; CHN analysis(%): $\text{C}_{14}\text{H}_{15}\text{ClN}_2\text{O}_3$; cal. C 57.05, H 5.13, N 9.50; found C 56.9, H 5.17, N 9.45.</p>
<div style="text-align: center;">  <p>(Table 2B.7, entry 6)</p> </div>	<p>5-Ethoxycarbonyl-6-methyl-4-(2,4-dichlorophenyl)-3,4-dihydropyrimidin-2(1H)-one 4f: Off white Solid, M.P.(°C): 247-249(248-250) [14]; FT-IR(KBr): 3360, 3220, 3105, 2971, 1697, 1644, 1591, 1456, 1370, 1322, 1297, 1226, 1096, 1047, 853, 816, 798, 653 cm^{-1}; ^1H NMR (400 MHz, DMSO-d_6): δ 9.28 (s, 1H), 7.72 (s, 1H), 7.35-7.52 (m, 2H), 7.26 (d, J = 8.3 Hz, 1H), 5.54 (s, 1H), 3.84 (q, J</p>

	<p>= 7.3 Hz, 2H), 2.25 (s, 3H), 0.96 (t, $J = 6.8$ Hz, 3H); ^{13}C NMR (100 MHz, DMSO-d_6): δ 165.3, 157.8, 151.7, 150.1, 141.5, 133.2, 130.8, 129.2, 128.5, 97.9, 59.7, 51.7, 18.2, 14.5; CHN analysis(%): $\text{C}_{14}\text{H}_{14}\text{Cl}_2\text{N}_2\text{O}_3$; cal. C 51.08, H 4.29, N 8.51; found C 51.03, H 4.60, N 8.47.</p>
<div style="text-align: center;">  <p>(Table 2B.7, entry 7)</p> </div>	<p>3,4-dihydro-4,6-diphenylpyrimidin-2(1H)-one 4g: White Solid, M.P.(°C): 245-247(244) [16]; FT-IR(KBr): 3335, 2379, 1651, 1531, 1225, 1050, 693 cm^{-1}; ^1H NMR (400 MHz, DMSO-d_6): δ 7.91 (s, 1H), 7.22-7.29 (m, 5H), 6.89-7.06 (m, 5H), 6.13 (brs, 1H), 5.60 (s, 1H), 4.22 (s, 1H); ^{13}C NMR (100 MHz, DMSO-d_6): δ 158.0, 154.8, 141.8, 137.3, 133.7, 129.2, 128.6, 128.4, 127.9, 127.3, 127.0, 126.4, 54.6; CHN analysis(%): Mol. formula $\text{C}_{16}\text{H}_{14}\text{N}_2\text{O}$, cal. C 76.78, H 5.64, N 11.19; found C 75.84, H 5.74, N. 11.21.</p>
<div style="text-align: center;">  <p>(Table 2B.7, entry 8)</p> </div>	<p>3,4-dihydro-4-(4-nitrophenyl)-6-phenylpyrimidin-2(1H)-one 4h: Off white Solid, M.P.(°C): 204-206(206-208) [16]; FT-IR(KBr): 3463, 3279, 1659, 1516, 1347, 1238, 1063, 849, 693, 597 cm^{-1}; ^1H NMR (400 MHz, DMSO-d_6): δ 8.14-8.19 (m, 3H), 7.45-7.55 (m, 3H), 7.18-7.26 (m, 2H), 6.88-6.94 (m, 1H), 6.18-6.27 (m, 1H), 5.72 (s, 2H), 4.29 (s, 1H); ^{13}C NMR (100 MHz, DMSO-d_6): δ 157.6, 155.8, 150.3, 146.5, 130.6, 127.3, 124.3, 123.3, 123.2, 58.7; CHN analysis(%): $\text{C}_{16}\text{H}_{13}\text{N}_3\text{O}$, cal. C 65.08, H 4.44, N 14.23;</p>

	found C 65.10, H 4.46, N 14.20.
<div style="text-align: center;">  <p>(Table 2B.7, entry 9)</p> </div>	<p>3,4-dihydro-4-(4-methoxyphenyl)-6-phenylpyrimidin-2(1H)-one 4i: White Solid, M.P.(°C): 202-204(201-202) [16]; FT-IR(KBr): 3248, 2933, 1676, 1612, 1508, 1456, 1338, 1248, 1173, 1028, 829, 769, 696, 556, 418 cm⁻¹; ¹H NMR (400 MHz, DMSO-d₆): δ 8.09-8.13 (m, 1H), 7.51-7.53 (m, 1H), 7.05-7.11 (m, 2H), 6.94 (s, 2H), 6.79-6.85 (m, 3H), 6.62 (d, <i>J</i> = 8.2 Hz, 2H), 6.55 (s, 1H), 4.18 (s, 1H), 3.61 (s, 3H); ¹³C NMR (100 MHz, DMSO-d₆): δ 162.6, 158.6, 154.8, 142.8, 133.8, 131.0, 128.2, 128.1, 127.8, 126.9, 113.9, 55.6, 54.1. CHN analysis(%): C₁₇H₁₆N₂O₂; cal. C 72.84, H 5.75, N 9.99; found C 72.88, H 5.80, N 9.96.</p>
<div style="text-align: center;">  <p>(Table 2B.7, entry 10)</p> </div>	<p>3,4-dihydro-4-(naphthalene-1-yl)-6-phenylpyrimidin-2(1H)-one (4j): Light brown Solid, M.P.(°C):204.2-206.2; FT-IR(KBr): 3362, 3051, 1667, 1608, 1522, 1385, 1281, 1173, 1145, 1116, 1031, 883, 769, 601 cm⁻¹; ¹H NMR (400 MHz, DMSO-d₆): δ 8.01 (d, <i>J</i> = 8.3 Hz, 1H), 7.90-7.92 (m, 1H), 7.84 (d, <i>J</i> = 8.2Hz, 1H), 7.45-7.59 (m, 4H), 6.85-6.89 (m, 1H), 6.73-6.74 (m, 2H), 5.57 (s, 4H); ¹³C NMR (100 MHz, DMSO-d₆): δ 157.9, 138.6, 133.9, 130.8, 129.0, 128.4, 126.7, 126.2, 125.7, 123.9, 123.1, 57.0; CHN analysis(%): C₂₀H₁₆N₂O; cal. C 79.98, H 5.37, N 9.33; found C 80.02, H 5.48, N 9.34.</p>

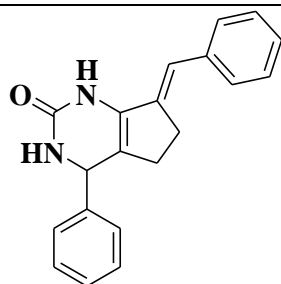


(Table 2B.7, entry 11)

(7E)-7-benzylidene-3,4,6,7-tetrahydro-4-phenyl-1H-cyclopenta[d]pyrimidin-2(5H)-one 4k: Yellow Solid, M.P.(°C): 235-236 (238-240) [15]; FT-IR(KBr): 3318, 3223, 3078, 2961, 1666, 1540, 1452, 1350, 1274, 1071, 752, 697 cm^{-1} ; ^1H NMR (400 MHz, DMSO- d_6): δ 8.79 (s, 1H), 7.21-7.35 (m, 11H), 6.59 (s, 1H), 5.11 (s, 1H), 2.74- 2.79 (m, 2H), 2.32-2.38 (dd, $J = 7.4$ Hz, 16.5 Hz, 1H), 1.92-1.98 (dd, $J = 6.4$ Hz, 16.9 Hz, 1H); ^{13}C NMR (100 MHz, DMSO- d_6): δ 153.8, 143.8, 139.7, 137.7, 136.4, 129.1, 129.0, 128.4, 128.0, 127.0, 126.6, 126.1., 119.1, 117.2, 57.9, 28.9, 28.8; CHN analysis(%): $\text{C}_{20}\text{H}_{18}\text{N}_2\text{O}$; C 79.44, H 6.00, N 9.26; found C 79.32, H 6.14, N 9.35.

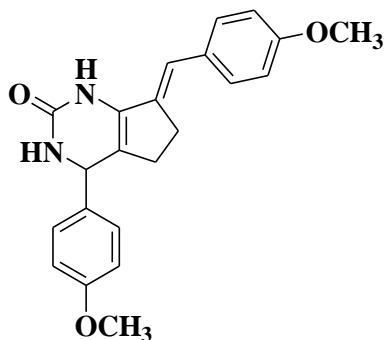


(Table 2B.7, entry 11)

(7E)-7-(4-methoxybenzylidene)-3,4,6,7-tetrahydro-4-(4-methoxyphenyl)-1H-cyclopenta[d]pyrimidin-2(5H)-one 4l: Brown Solid, M.P.(°C): 256-258 (254-257) [15]; FT-IR(KBr): 3372, 3210, 3113, 2931, 2836, 1686, 1603, 1511, 1449, 1349, 1247, 1176, 1026, 890, 820, 753, 526 cm^{-1} ; ^1H NMR (400 MHz, DMSO- d_6): δ 8.6 (s, 1H), 7.23 (d, $J = 8.7$ Hz, 2H), 7.14 (d, $J = 8.7$ Hz, 2H), 7.06(s, 1H), 6.86-6.89 (m, 4H), 6.51 (s, 1H), 5.03 (s, 1H), 3.74 (s, 6H), 2.70-2.75 (m, 2H), 2.27-2.33 (dd, $J = 6.4$ Hz, 16.9 Hz, 1H), 1.91-1.97 (dd, $J = 6.0$ Hz, 17.4 Hz, 1H); ^{13}C NMR (100 MHz, DMSO- d_6): δ 159.1, 158.1, 153.7, 137.3, 136.3, 136.1, 130.9, 129.7,

	128.2, 118.0, 116.6, 114.5, 114.4, 57.3, 55.6, 28.7. CHN analysis(%): C ₂₂ H ₂₂ N ₂ O ₃ , cal. C 72.91, 6.12, N 7.73; found C 72.89, H 6.18, N 7.77.
--	--

References

1. Davis, M. E. Zeolites and molecular sieves: not just ordinary catalysts. *Industrial & Engineering Chemistry Research*, 30(8):1675-1683, 1991.
2. Gogoi, P., Dutta, A. K., Sarma, P., and Borah, R. Development of Brønsted-Lewis acidic solid catalytic system of 3-methyl-1-sulfonic acid imidazolium transition metal chlorides for the preparation of bis (indolyl) methanes. *Applied Catalysis A: General*, 492:133-139, 2015.
3. Dutta, A. K., Gogoi, P., and Borah, R. Synthesis of dibenzoxanthene and acridine derivatives catalyzed by 1, 3-disulfonic acid imidazolium carboxylate ionic liquids. *RSC Advances*, 4(78):41287-41291, 2014.
4. Flanigan, E.M., Khatami, H., and Szymanski, H.A. Infrared structural studies of zeolite frameworks, In *Molecular Sieve Zeolites-I*, volume 101 of *Advances in Chemistry*, chapter 16, pages 201–229, ISBN13: 9780841201149, American Chemical Society, Washington, DC.
5. Yan, Z., Ma, D., Zhuang, J., Liu, X., Liu, X., Han, X., Bao, X., Chang, F., Xu, L., and Liu, Z. On the acid-dealumination of USY zeolite: a solid state NMR investigation. *Journal of Molecular Catalysis A: Chemical*, 194(1):153-167, 2003
6. Covarrubias, C., Quijada, R., and Rojas, R. Ethylene polymerization using dealuminated ZSM-2 zeolite nanocrystals as an active metallocene catalyst support. *Applied Catalysis A: General*, 347(2):223-233, 2008.
7. Rüscher C.H., Buhl, J. C., Lutz, W., Galarneau, A., Di Renzo, F., Fajula, F., and Vedrine, J. *Studies in Surface Science and Catalysis*. Elsevier, Amsterdam, volume 135:13-15, 2001.
8. Senderov, E., Halasz, I., and Olson, D. H. On existence of hydroxyl nests in acid dealuminated zeolite Y. *Microporous and Mesoporous Materials*, 186:94-100, 2014.

9. Grobet, P. J., Jacobs, P. A., and Beyer, H. K. Study of the silicon tetrachloride dealumination of NaY by a combination of nmr and ir methods. *Zeolites*, 6(1):47-50, 1986.
10. Fejes, P., Hannus, I., Kiricsi, I., Pfeifer, H., Freude, D., and Oehme, W. Thermal stability of hydroxy groups in dealuminated mordenites. *Zeolites*, 5(1):5-48, 1985.
11. Voogd, P., Scholten, J. J. F., and Van Bekkum, H. Use of the t-plot-De Boer method in pore volume determinations of ZSM-5 type zeolites. *Colloids and Surfaces*, 55:163-171, 1991.
12. Thomazeau, C., Olivier-Bourbigou, H., Magna, L., Luts, S., and Gilbert, B. Determination of an acidic scale in room temperature ionic liquids. *Journal of the American Chemical Society*, 125(18):5264-5265, 2003.
13. Ghomi, J. S., Teymuri, R., and Ziarati, A. A green synthesis of 3, 4-dihydropyrimidine-2 (1H)-one/thione derivatives using nanosilica-supported tin (II) chloride as a heterogeneous nanocatalyst. *Monatshefte für Chemie-Chemical Monthly*, 144(12):1865-1870, 2013.
14. Ahn, B.J., Gang, M.S., Chae, K., Oh, Y., Shin J., and Chang, W. A microwave-assisted synthesis of 3,4-dihydro-pyrimidin-2-(1H)-ones catalyzed by FeCl₃-supported nano pore silica under solvent-free conditions. *Journal of Industrial and Engineering Chemistry*, 14(3):401-405, 2008.
15. Tu, S., Fang, F., Miao, C., Jiang, H., Feng, Y., Shi, D., and Wang, X. One-pot synthesis of 3, 4-dihydropyrimidin-2 (1H)-ones using boric acid as catalyst. *Tetrahedron letters*, 44(32):6153-6155, 2003.
16. Phukan, M., Kalita, M. K., and Borah, R. A new protocol for Biginelli (or like) reaction under solvent-free grinding method using Fe (NO₃)₃.9H₂O as catalyst. *Green Chemistry Letters and Reviews*, 3(4):329-334, 2010.
17. CCDC-1507118 (**4f**) contains the supplementary crystallographic data for this paper. This data can be obtained free of charge from the Cambridge Crystallographic Data Centre via http://www.ccdc.ac.uk/data/_request/cif.